2013

Viscosity Regulation in Polymer Extrusion

Diane K. Haberbusch
Cleveland State University

VISCOSITY REGULATION IN POLYMER EXTRUSION

DIANE K. HABERBUSCH

Bachelor of Science in Mechanical Engineering

Case Western Reserve University

May 1993

submitted in partial fulfillment of requirements for the degree

MASTER OF SCIENCE IN ELECTRICAL ENGINEERING

at the

CLEVELAND STATE UNIVERSITY

December 2013

We hereby approve this thesis for

Diane K. Haberbusch

Candidate for the Master of Science in Electrical Engineering degree for the

Department of Electrical and Computer Engineering

and the CLEVELAND STATE UNIVERSITY

College of Graduate Studies

Thesis Chairperson, Zhiqiang Gao

Department of Electrical and Computer Engineering, December 4, 2013

Thesis Committee Member, Lili Dong

Department of Electrical and Computer Engineering, December 4, 2013

Thesis Committee Member, Orhan Talu

Department of Chemical and Biomedical Engineering, December 4, 2013

Student's Date of Defense: December 4, 2013

ACKNOWLEDGEMENTS

Thank you to my advisor, Dr. Zhiqiang Gao, for sharing his knowledge and for supervising my work on this thesis. His guidance and inspirational insights have helped make this project meaningful to me.

Thanks to my committee, Dr. Lili Dong and Dr. Orhan Talu, for reviewing this thesis and for giving their input. Thanks also to Dr. Dong for teaching key concepts.

Thank you to Dr. Joseph Golba and Dr. Eddie Geng of PolyOne Corporation, and to their colleagues, for their time and energy in letting me observe an extruder in operation and for answering my questions.

Thank you to my friends at Cleveland State University, Gregg Calhoun, for donating time, energy, and equipment; Qinling Zheng, Han Zhang, Xiaoxu Li, and Jason Tatsumi for their help with this thesis and for answering my questions.

Thanks to Adrienne Fox and Jan Basch, in the Electrical and Computer Engineering Department at Cleveland State University, for their help through the years.

Thanks to my husband, Mark, for his help and encouragement. Thanks to Matthew, Karen, and the rest of my family for their support.

VISCOSITY REGULATION IN POLYMER EXTRUSION

DIANE K. HABERBUSCH

ABSTRACT

The interesting background and history of polymer extrusion are first introduced in this thesis. The complexity of the extrusion process is described, along with sources of disturbances. A literature review of the types of controllers that have been used for viscosity regulation in polymer extrusion is given, including the proportional-integral-derivative (PID) proportional-integral (PI) controllers. Polymer viscosity in extrusion is difficult to model accurately and its regulation is prone to disturbances. Active Disturbance Rejection Control (ADRC) is the right method for addressing the model inaccuracies and facilitates a straightforward solution to accommodate industrial needs with parameters that can be easily tuned by the operator. To do this, first the problem of viscosity regulation has to be reformulated as a disturbance rejection problem. This thesis demonstrates, using a circuit and simulation, an advanced solution. The initial results are encouraging, showing better control than PI.

TABLE OF CONTENTS

TABLE OF FIGURES

CHAPTER I

INTRODUCTION

Extruders are widely used in the commercial polymer processing industry. In some processes, the extruder is used to mix ingredients and extrude a compound polymer, which will be cooled, chopped, and sold in pellet form. Other processes involve extrusion of a hose or film that requires control of a thickness or another dimension of the extrudate. The extruder may be one step in the process of blow molding or injection molding. In all of the uses of the extruder, there is a need to regulate more than one variable of the extrusion process. Barrel temperatures in different zones of the extruder, along with die temperature, are process variables that need to be controlled in all cases of extrusion. Die pressure is a controlled process variable [1-2] when a die valve is present. In industry, the controlled quality variable may be the dimension of the extrudate [1, 3-6] after it exits the die or viscosity of the polymer upstream of the die [7-14].

The focus of this thesis is on regulation of viscosity in polymer extrusion. In viscosity regulation in continuous extrusion, the viscosity may be directly measured through on-line measurement or calculated with real-time measurement of viscosity variables [8-12]. The viscosity of the polymer melt at the screw tip of the extruder varies due to disturbances during the extrusion process. These disturbances are due to changes in grade of ingredients, variation in operation of extruder equipment and auxiliary devices, and dynamics of the solid and melt flow within the extruder [7]. In processes in which a chemical reaction takes place in the melt, commonly called reactive extrusion (REX), another disturbance is the variation in the composition of the polymer ingredients. The inability to respond to disturbances during a production run of the extruder can result in off-specification product and down-time [7].

1.1 Background

The three main categories of polymers are elastomers, thermosets, and thermoplastics. A thermoplastic material will melt when heated and solidify when cooled. A typical thermoplastic may be reheated and reformed after it has been cooled, whereas all thermosets and most elastomers go through an irreversible chemical change during the forming process. A thermoset undergoes an irreversible crosslinking of molecules when heated above a certain temperature at a given pressure. Most elastomers, which include rubber compounds, will vulcanize when heated above a certain temperature at a given pressure. Vulcanization is the process of crosslinking in elastomers, and occurs above a certain temperature. During the mixing and preforming of elastomers and during the

extrusion and molding of thermosets, it is important to stay below the temperature that causes crosslinking to occur for the specific polymer or polymer compound.

The control of process variables during polymer mixing, extrusion, blow molding, and injection molding is necessary to maintain high product quality. The controls of melt temperature, extruder barrel pressure, and mold cavity pressure in the case of blow molding, are important for thermosets and elastomers to ensure that the vulcanization or crosslinking does not occur until the appropriate time during the final forming process [15]. For the extrusion process of any polymer, there are typically many variables that need to be regulated. These variables, and how they relate to each other and to viscosity, will be explained in the next section following a discussion of the physical description of a polymer extruder.

An extruder forces material through a die. There are two categories of polymer extrusion: continuous and discontinuous. A continuous operation single screw extruder has one rotating member that transports the polymer along the axis of a barrel and through the die. A multi-screw extruder has more than one rotating member. A discontinuous extruder has a reciprocating member that pushes the polymer out of the die intermittently. This type of extruder is used for processes such as injection molding and blow molding. The continuous extruder may be used for blow molding if an accumulator reservoir is located at the exit of the extruder barrel and if there are moving molds on the production line. Otherwise, an electro-hydraulic ram is employed for injection and blow molding with a reciprocating screw extruder, such that the rotating extruder also moves linearly due to the pressure exerted by the ram.

The plasticating single screw extruder is the most common type of extruder used in the polymer processing industry [16]. Plasticating extrusion is a term for a process in which the polymer is fed from a hopper into the feed port of the extruder in solid form and melted as it is conveyed through the barrel to the die. In this process, the extruder performs two operations. The first operation is melting, and the second operation is developing pressure to force the polymer through the die. If mixing is to be done in the extruder, the extruder may resemble the plasticating extruder and also have a tube connected to the feed port for injection of a liquid, or a second hopper over the feed port for gravity feeding of an additional ingredient in solid pellet form.

A plasticating extruder has three process zones. These zones are the solids conveying, melting, and melt conveying zones. The zones are shown in Figure 1.1. The melt conveying zone is also referred to as the pumping zone. Along with a hopper and feed port, the plasticating extruder typically has controlled temperature barrel zones and a die through which the polymer is forced. In Figure 1.1, the transport of the polymer is from left to right. The labeled parts of the extruder are included in Figure 1.2 and Figure 1.3. The transport of material is from right to left in Figure 1.2, and from left to right in Figure 1.3. The removable breaker plate, also called a screen pack, shown in Figure 1.2, holds the mesh screens that trap contaminants before the polymer is pushed through the die.

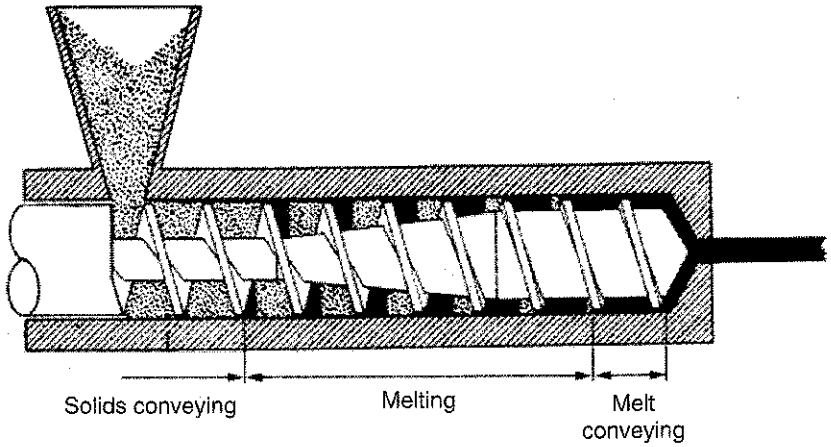

Figure 1.1 Typical screw geometry of a plasticating extruder [7]. Copyright by *SAGE Publications*. Reprinted with permission.

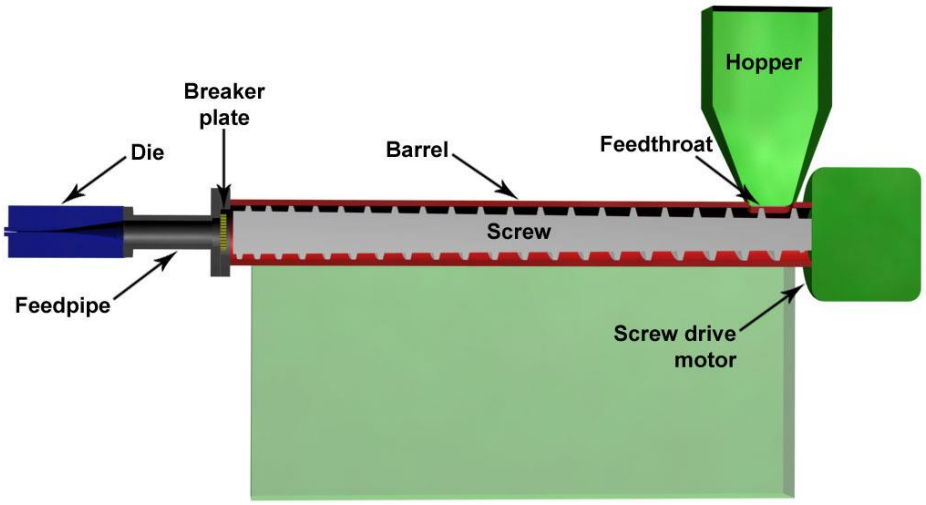

Figure 1.2 Labeled diagram of a single screw extruder [17].

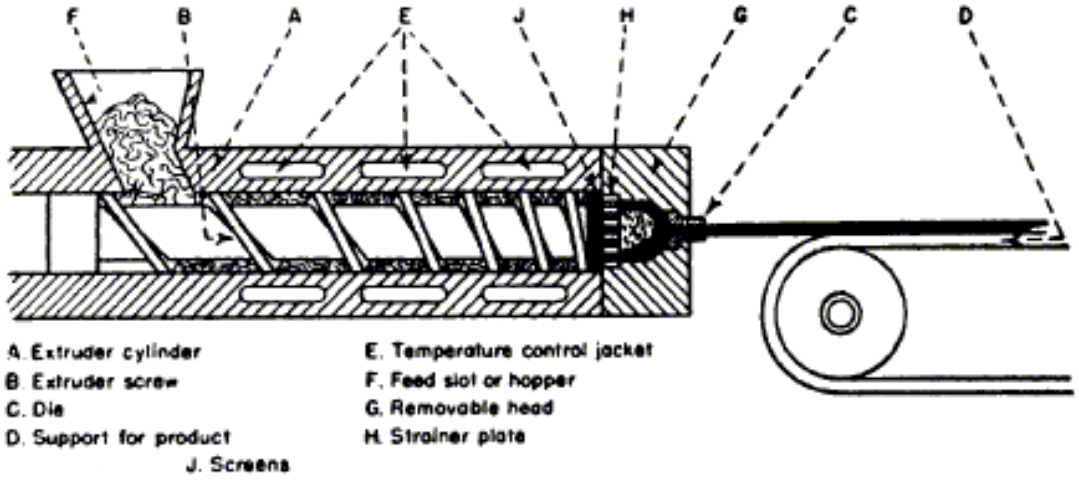

Figure 1.3 Labeled diagram of a single screw extruder used in the 1940s [18]. Copyright by *Society of Plastics Engineers, Inc.* Reprinted with permission.

Many extruders have thermocouples inserted into the barrel at each barrel zone to measure the barrel temperature, and at the die to measure the die temperature. An extruder typically has more than three barrel zones that are temperature regulated [1, 19]. In many processes, cooling is needed for barrel zone temperature control. The cooling is accomplished with a cooling fan below or a water cooling line within the barrel at each temperature zone along the extruder. Some screws have a hollow interior so that water or oil may be circulated inside the screw and through a heat exchanger to provide additional cooling of the polymer in the extruder. In terms of energy cost, it is desirable to maintain temperature in the barrels without undershoot and overshoot of the temperature [19].

In terms of part quality, the manipulation of the barrel zone temperature and die temperature has been found to be of importance due to the dependence of viscosity on temperature [7, 16, 20]. Viscosity is also dependent on shear rate. The shear rate of the polymer caused by the rotating screw and the stationary barrel is characterized by the

screw geometry and screw speed for a single screw extruder [7, 11, 20]. Also, the polymer temperature inside the barrel increases with an increase in screw speed, and decreases with a decrease in screw speed due to the increase or decrease in shearing of the polymer by the screw. The pressure of the melt inside the barrel is also a coupled parameter with temperature: a change in polymer temperature causes a change in pressure within the barrel and a change in pressure causes a change in polymer temperature [9, 10, 13]. In some cases the pressure inside the barrel near the die is a measured variable that is used for a real-time calculation of viscosity [2, 3, 6]. All extruders have a pressure transducer located upstream of the die, at the screw tip. Some extruders have a die restrictor valve. A die restrictor valve will allow manipulation of the pressure inside the extruder. Due to the inter-relationship of temperature, pressure, and viscosity, a manipulation of a die restrictor valve will cause a change in pressure, temperature, and viscosity of the polymer melt.

There are additional coupled parameters in REX besides the coupled parameters already mentioned for extrusion. In REX, the polymer melt flow, temperature, and reaction are coupled [21-22]. The temperature and reaction are coupled through activation energy and enthalpy. The activation energy, which is a variable in the kinetic model of the chemical reaction, is a function of temperature. The enthalpy is based on the heat and energy of the reaction. Temperature and flow are coupled through viscosity, heat transfer, and heat generation. The chemical reaction and flow are coupled through viscosity and residence time. The residence time is the time that the polymer is in the extruder, and is a function of the screw speed and the polymer melt flow.

Many REX processes involve the use of an initiator, usually peroxide. There are several grades of peroxide, and each grade has a half-life. The peroxide half-life is specified in the commercial data sheet of the peroxide grade for a given temperature. The half-life depends on the temperature at which the reaction occurs. An increase in temperature of the polymer melt in the extruder, caused by changes in barrel temperature, increase in screw speed, or increase in pressure will cause a given product and grade of initiator to degrade faster. A faster degradation of the initiator or a change in grade of the initiator ingredient adds to the uncertainty of the process dynamics. In a reactive extrusion process, any external disturbances or changes in the process dynamics may cause undesired changes in the kinetic reactions that occur in the extruder.

It is extremely difficult to use first-principle methods to model the dynamics of extrusion from physical considerations [4, 7-8, 23]. The mathematical descriptions of the process dynamics are complex [23], and the viscosity of polymers is nonlinear with change in screw speed and temperature. The inter-relationships between the viscosity, screw speed, temperature, and pressure, along with the complexity of the mathematical descriptions of the process dynamics present a challenge for accurate dynamic modeling of the extrusion process. There are also several load variables in viscosity regulation, depending on the choice of the manipulation variable, which may present disturbances.

Research in viscosity regulation in polymer extrusion has focused on algorithms of the PI (Proportional-Integral) and PID (Proportional-Integral-Derivative). These algorithms include self-tuning regulator [5], minimum variance [5, 10, 13], Smith predictor [6], genetic [9], fuzzy scheduling [9, 11], constrained minimum variance [13], and pole placement [13]. Most of the models developed in viscosity regulation research

were developed empirically. The empirical model that is developed for a given extrusion process is dependent on the polymer grade and the operating range of the specific equipment.

1.2 History of Extrusion

The extruder screw was invented around 225 B.C. for the purpose of moving water from the inside of a leaking ship to the outside of the ship. The name of the invention is *Cochlea Archimedis*, and was invented by Archimedes in Syracuse for his employer, King Hiero [24]. The extruder screw design was later used by Egyptians for irrigation purposes. The current of the river turned the screw, which caused the water to be lifted. The illustration of the design is shown in Figure 1.4.

The scientific principles of fluid flow near a flat plate were developed by C. Navier in 1582, J. Poiseuille in 1842, M. Boussinesq in 1868, and O. Reynolds in 1886, which all contributed to the explanation of a model of fluid flow with the Archimedean screw [24]. All of these principles were initially developed for Newtonian fluids, such as water. The analyses of extrusion of non-Newtonian fluids, which include molten rubbers and plastics, were first published in 1922 [16]. The first extruders invented for polymer extrusion were intended for rubber extrusion, and used steam to heat the barrels.

Invention of the first single screw extruder for polymer extrusion is attributed to Matthew Gray of London, England, in 1879 [15]. The purpose of the extruder was to extrude rubber compounds and gutta percha through extrusion shaping dies. Michael

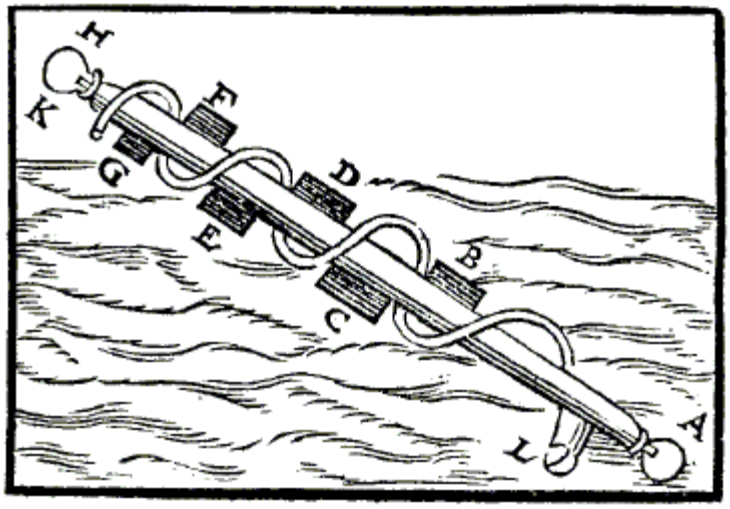

Figure 1.4 The *Cochlea Archimedis* used to lift water from the Nile [18]. Copyright by *Society of Plastics Engineers, Inc*. Reprinted with permission.

Faraday recommended gutta percha for copper cable insulation in a letter to Richard Phillips, published in *The London, Edinburgh, and Dublin Philosophical Magazine and Journal of Science* in March 1848 [25]. The popularity of gutta percha insulation grew with its early implementation as a telegraph wire insulator, and later as insulation for underwater cable. Matthew Gray specifically stated that his machine would apply to wire coating for the purpose of insulating electrical wires [24, 26]: "*The object of the present invention is to supply india rubber, gutta percha, and similar plastic compounds to moulding or shaping dies, free of air and comparitively free of moisture, and that at a uniform or unvarying pressure."* [26] Figure 1.5 is a drawing from his 1879 patent application of a wire coating extruder.

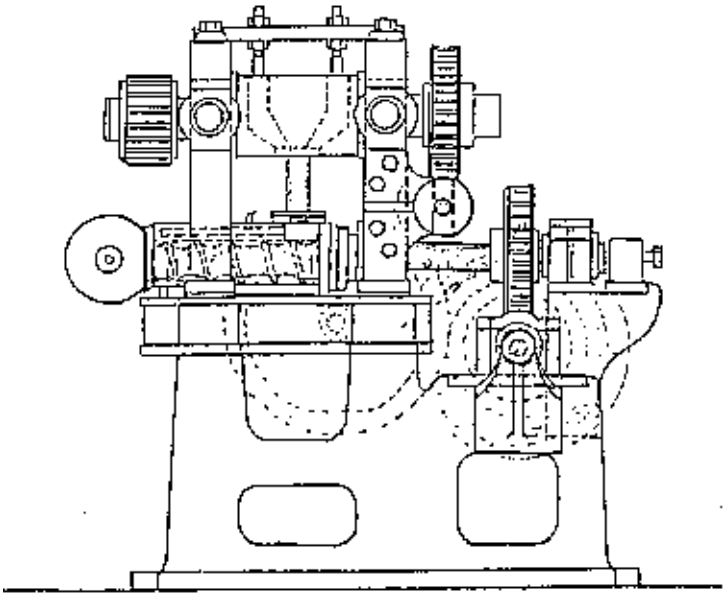

Figure 1.5 Drawing of Matthew Gray's wire insulation extruder [26].

John and Vernon Royle were granted a patent for their single screw extruder rubber tubing machine in 1933. *Royle and Son's* single screw extruder was manufactured commercially in Paterson, New Jersey [27]. A sketch from the patent application is shown in Figure 1.6. Francis Shaw of Manchester, England, also patented a commercial single screw extruder around the same time [27].

Prior to 1879, Francis Shaw worked for *Charles Macintosh and Company*, before he started his own company, *Francis Shaw and Company Ltd*. *Charles Macintosh and Company* came into operation in 1825, and supplied mixers, also called masticators, for the mixing and kneading of rubber compounds. The early patents for polymer mixers were filed by Thomas Hancock, who invented the first single rotor masticator in 1820, and Edwin Chaffee, who filed the patent for the two roll mill in 1836 [24]. In 1846, Thomas Hancock patented the first molding machine for rolled sheets of rubber, a

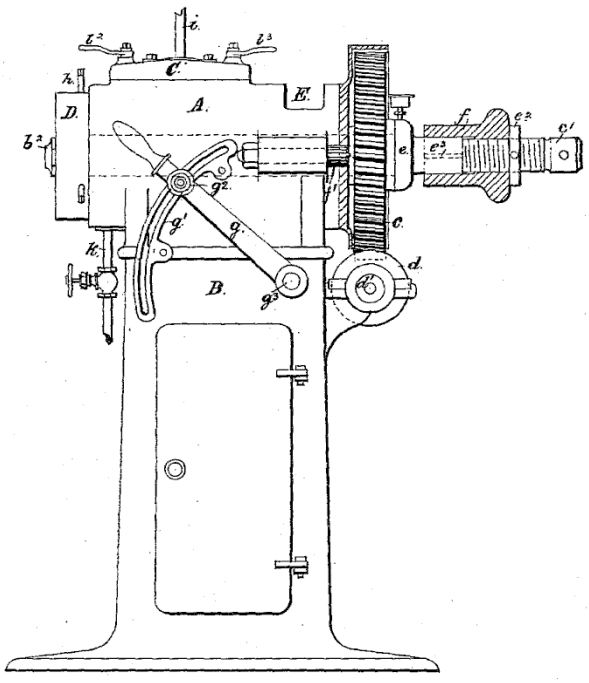

Figure 1.6 Drawing of John and Vernon Royle's single screw extruder [28].

precursor to the blow molding and injection molding machines. By 1880, twin rotor masticator-mixers were patented in the food industry for butter churning and kneading of bread dough. Mixing of natural rubbers was done in an open two roll mill prior to the development of a toxic organic amine accelerator. The use of the accelerator in the rubber compound to speed the vulcanization process for pneumatic tire production required enclosed mixing, hence the invention of the internal mixer.

The first twin screw extruders were described in a patent in 1869 by Francois Coignet for the processing of artificial stone paste. At the same time, extruders were invented and used in the food, soap, and metal industries [27]. Around 1935, a twin screw extruder was developed by Roberto Colombo in Italy [16] for polymer extrusion. Colombo worked with Carlo Pasquetti on mixing cellulose acetate. Colombo developed

an intermeshing co-rotating twin screw extruder, while Pasquetti developed an intermeshing counter-rotating twin screw extruder. Colombo's extruder design was patented, and the rights were purchased by many companies.

A single screw extruder that was electrically heated for thermoplastics was designed by H. Heidrich in 1935. Prior to 1935, the barrel of the single screw extruder was typically heated with steam. *Paul Troester Mascshinenfabrik Gmb*, in Germany, began to commercially sell an electrically heated single screw extruder in 1940. This was a single screw extruder of longer length to diameter (L:D) ratio than the elastomer extruders used earlier than 1935. *Troester* built single screw extruders in Hannover, Germany beginning in 1892. *Hermann Bertorff* also produced screw extruders in the 1890s [27]. *Maschinenefabrik Paul Leistritz GmbH* began producing twin screw extruders commercially in Germany in the 1930s. In 1939, low density polyethylene, which is a thermoplastic, was developed. This spurred further development of the blow molding machine. In 1950, *Continental Can* was issued a patent for a continuous extrusion blow molder. *Continental Can* and *Plax* were the only two American companies that held patents in the early half of the 1950s. Development of high density polyethylene in 1953 further increased growth in blow molding in the second half of the 1950s, mainly in Europe [29].

The discipline of polymer processing emerged by the 1950s with developments in science and technology. The first set of scientific analyses of polymer extrusion on a single screw extruder were conducted in the early to mid-1950s and published in 1953 through 1959 by J. F. Carley, R. A. Strub, R. S. Mallouk, J. M. Kelvey, and E. C. Bernhardt of du Pont [27, 30]. A study of the melting mechanism in single screw

extruders was conducted by Bruce Maddock in 1959 [30-31]. Soon after, a mathematical description of the melting mechanism was completed and verified by Zehev Tadmor [23].

Tadmor's mathematical description has been incorporated into research control algorithms that involve recursive solutions of steady-state equations of conservation of energy and mass until a best guess of flow rate or viscosity is determined through convergence of dynamic pressure profile and dynamic solid bed profile calculations [4, 7, 9, 23]. The solid bed profile is amount of solid pellet in the screw channel as the polymer travels along the helical channel length along the extruder. The transient equations cannot be solved due to the unavailability of the values of the changing density, specific heat, and heat transfer coefficient of the melt during the melting process in the extruder barrel. In industry, the computer simulation software applications that exist at the present time are used to design screw geometry for single and twin screw extruders rather than for control models of the extrusion process for a given polymer. An REX process is even more complex than Tadmor's mathematical description, due to the exothermic property and temperature dependence of the kinetic reactions occurring in a given REX process.

1.3 Motivation

The melting and melt conveying mechanisms in a plasticating single screw extruder consist of several dynamic transport processes. The conservation of energy and the conservation of mass are the physical laws that are the basis of melting and melt conveying in an extruder. Transient equations of the temperature profile and solid bed

profile in the extruder cannot be solved without recursive method due to unavailability of polymer properties for a given temperature or viscosity. For example, the heat transfer coefficient is one of the properties that changes with the changing viscosity along the extruder barrel, and is required to solve a transient equation of the solid bed profile. Algorithms used in computer aided engineering tools are based on steady-state equations of the temperature and solid bed profiles, and are used in industry for extruder screw design, not for regulation of the quality of the polymer melt.

The inter-relationships of variables and the complexity of the mathematical descriptions of the process dynamics present a challenge for accurate dynamic modeling of the extrusion process, which in turn presents a challenge for regulation of viscosity. The disturbances to viscosity are also varied and cannot be modeled accurately. The method of Active Disturbance Rejection Control (ADRC) estimates the disturbance along with the change in process dynamics, through the use of an extended state observer, and provides a solution for controlling a process in which process variables are coupled and process dynamics are uncertain.

1.4 Thesis Organization

The literature review of viscosity models and controller algorithms is presented in Chapter II. The mass and energy equations of viscosity, along with the problem description and reformulation of the plant model are given in Chapter III. Simulations of the PI and the ADRC algorithms are presented and compared in Chapter IV.

Experimental results of PI control and ADRC of the circuit-simulated plant are given in Chapter V. Conclusions and future work are given in Chapter VI.

CHAPTER II

LITERATURE REVIEW

In this chapter, literature review on the models used for control of polymer extrusion variables such as flow rate, extrudate dimension, pressure drop, temperature, and viscosity is provided in Section 2.1. Types of controller algorithms used in polymer extrusion are listed in Section 2.2. A literature summary of the Active Disturbance Rejection is given in Section 2.3. A summary of the literature review is given in Section 2.4.

2.1 First-Principle and Empirical Models

McAfee [7] discusses the use of empirical and first-principle models in polymer extrusion control. The first-principle models developed in polymer extrusion give a

physical understanding to an extrusion process, but involve complex, coupled partial differential equations that require recursive solutions. The differential equations are based on conservation of mass and energy [7, 31]. Computer software has been developed to aid in solutions of the differential equations that result in steady-state pressures and temperatures, but require information about the material's frictional, thermal, and rheological properties that may be unknown, change with material grade, or change with extrusion dynamics [7, 31]. Also, these computer software programs are usually used off-line and only for initial design of the extruder or the process. McAfee states, *"There is therefore a need for extrusion models which can be run on-line to enable control of disturbances and optimization of settings for individual material properties."* [7] (Copyright by *SAGE Publications*. Reprinted with permission).

McAfee proposes "grey box" modeling based on physical knowledge of the system with the use of a black box technique to tune unknown parameters [7]. This technique is similar to that of Previdi *et al.* [1], who uses a first principle model of the extruded polymer flow rate, published by Rauwendaal [16], along with transfer functions empirically determined for step changes in barrel temperature and screw speed in order to develop models for extrudate dimension control. Kochhar *et al.* [4] and Previdi *et al*. [1] found a more rapid response to a change in die pressure set-point than to a change in melt temperature set-point. Previdi's experimental results show a time constant of approximately 30 minutes for a step change in barrel zone temperature. A faster change in melt temperature can be accomplished with screw speed and die restrictor valve manipulations than with barrel zone temperature manipulation [4].

Chen et al. [20] also combine a first-principle technique with an empirical model for viscosity calculation based on melt temperature and screw speed. They use an in-line capillary rheometer to measure viscosity and incorporate a first-principle flow equation for the shear rate as a function of the flow rate through the rheometer in their model. Chen *et al*. use the power-law equation of viscosity in the development of their model and assume that the power law index of the polymer is constant. Due to this assumption, an error exists between the calculated viscosity and the measured viscosity. Experimental measurements of polypropylene viscosity at three different temperatures, each at five different screw speeds, were compared to the model calculation of viscosity for the respective temperatures and screw speeds. The curves for the viscosity versus screw speed for given temperatures were of similar shape for the experiment and the model. A shift of the curve of the model data on the plot of viscosity versus screw speed has to be made in order to line up the results of the model with the experiment, and this shift depends on the operating melt temperature.

Due to the complexity of the mathematical description of the melt profile and pressure profile along the extruder, "black-box" empirical models are the most prevalently used models in polymer extrusion feedback control research. Empirical models are obtained experimentally using either step response methods or pseudo-random binary sequence inputs. Both methods are based on strict operating materials, plant set-up, and ranges of variables for operation. Changes to any of these would require a change to the model, which is difficult to apply intuitively because of the lack of physical meaning. Empirical models that have been developed in polymer extrusion

control include Broadhead *et al.* [10], Chiu *et al.* [11], Pabedinskas *et al.* [12-13], Kochhar *et al.* [4], Costin *et al.* [5] and Yang *et al.* [6].

Chiu and Pong [11] studied viscosity control of an unspecified grade of low density polyethylene (LDPE) with screw speed as the manipulation variable. Screw speed manipulation has been shown to have a relatively short time constant compared to the input step response of other process variables. For example, the manipulation of barrel temperature may have a time constant on the magnitude of ten minutes [1, 4] whereas the manipulation of screw speed has a time constant less than one minute. A second order model was developed empirically by Chiu and Pong through step response tests. The viscosity control using a traditional PID algorithm was compared to their proposed fuzzy scheduled gain algorithm of a PID controller. The fuzzy scheduled gain controller was found to have a quicker response with less oscillation of the controller output for a specified set-point change. Notably, the fuzzy scheduling of a PID is based on the material, equipment, and operating conditions. Changes in any of these will require determination of new parameters of the fuzzy scheduling.

Pabedinskas *et al.* [12-13] proposed and compared simulations of three PID controller algorithms for the regulation of viscosity in controlled degradation of polypropylene (CRPP): minimum variance (MV), constrained minimum variance (CMV), and pole placement (PP). The manipulated variable in [13] is the feed peroxide concentration. The peroxide is an initiator of the chemical reaction; it is used as a source of free radicals for the degradation reaction. An empirical model of viscosity was developed by Pabedinskas *et al.* [13] with step increases and step decreases in peroxide concentrations from various initial concentrations. This was done with specified

equipment at specified operating conditions. Most step response data were generated with one grade of polypropylene. A second grade of polypropylene was used for some step response data in order to consider the disturbance of the variation of feed properties. It was found in [13] that a SISO (Single-Input-Single-Output) relationship of peroxide concentration as the input and viscosity as the output in the degradation of polypropylene process can be described by a first-order plus dead-time transfer function model. The dead time of the process is the sum of the residence time of the process plus the sensor measurement delay. The residence time is the length of time for the polymer to travel from the feed throat to the exit of the extruder.

Several observations listed in [13] are: 1) the process gain is nonlinear, 2) the process gain is different between two grades of feed materials, and 3) the gain is smaller for decreases in the initiator concentration than for increases in the concentration in the same concentration range. Dead time, nonlinear process gain, and different process gains for upward and downward steps were also found in [10] for the manipulation of the injection of an ingredient in the reactive extrusion of a different polymer. In the case of controlled degradation of polypropylene, the last observation was hypothesized to be due to the residual peroxide in the extruder, supported by the fact that the difference in the gains for step increases and step decreases was greater in the higher peroxide concentration range. The changes in process time constant and dead time did not follow a pattern

In simulations, the MV and CMV did not prove to be robust for mismatches in model and actual delay time. The PP controller was found to deal better with dead time mismatch in simulation, and was therefore implemented in an experiment with the

process. The viscosity oscillated when the feed material grade was changed slightly. Pabedinskas *et al.* speculate that this oscillation is due to the mismatch between the model and actual process gain because the oscillation did not occur when the feed material was switched back to the original grade ingredient.

2.2 Controller Algorithms

A variety of PID controller algorithms have been proposed for viscosity regulation in the research community. These algorithms include self-tuning regulator (STR) [5], MV [5, 10, 13], Smith predictor [6], genetic [9], fuzzy scheduling [9, 11], CMV [13] and PP [13]. The performance of some of these controller algorithms were compared to that of a traditionally tuned PID or PI algorithm. In their performance studies, some included the addition of a disturbance in their simulations or experiments, and only a few considered changing the disturbance and the process dynamics [5-6, 12-13].

A PID has three gains, K_P, K_I, and K_D, that each act upon the error until the set-point is eventually achieved. The PID does not work well for disturbance rejection if the level or type of disturbance is unknown, or if a change in process dynamics, for which it has been tuned, has occurred. The complexity of the first-principle model, and its requirement of changing frictional, thermal, and rheological properties of the material in order to solve for an accurate transient description, has made it impossible for researchers and commercial manufacturers to implement any of the above PID algorithms without

tuning parameter gains through simulation or experimentation for specific materials at specific operating conditions on specific equipment.

In order for viscosity control to be implemented more widely in industry, a method that follows a general approach is needed. This method must not require an accurate knowledge of the transient behavior for the specific polymer and process. This method must also incorporate a method for regulation of viscosity in the presence of any disturbances or changes in the dynamics. ADRC is a method that meets these requirements.

2.3 Active Disturbance Rejection

The technique of ADRC was originally conceptualized and proposed with a nonlinear structure by J. Han [32-33], and later simplified and parameterized in [34]. A unique state observer is utilized in the method to estimate what is called the general disturbance. The general disturbance includes the output disturbance and the change in the internal process dynamics from the ideal internal process dynamics. This is achieved with an observer that tracks an extended state of the state space model. This observer is called an Extended State Observer (ESO). The state space model of the plant only has to include an estimate of the model. The estimation may be a linear state space model of a nonlinear process. The general disturbance is tracked with a well-tuned observer [34] and then cancelled in the control law.

The decoupling problem is reformulated as that of disturbance rejection. An input-output pairing may be used in this technique, and the effect of one input to all other

outputs that it is not paired with is viewed as a disturbance. The disturbance is estimated using the ESO. The cancellation of this disturbance in the control law by ADRC leads roughly to a set of single-input and single-output processes to be controlled. A set of singe-input and single-output processes are much easier to control than a multivariable relationship of inputs and outputs.

Temperature control is one example in which ADRC offers a solution for process control where there is a coupling of variables. In barrel temperature zone control, the adjacent zones have an inter-relationship. ADRC is currently in use in programmable logic control code on multiple production lines of polymer hose extruders for temperature control of each barrel zone [19]. Its implementation saved energy costs compared to the formerly existing control system that was used by the manufacturer. Originally, the hose manufacturer used a traditionally tuned PID controller in each of the seven barrel zones of the extruder to control the zone temperatures. Heat was added to a zone with a heater relay command. If the temperature of the zone exceeded the set point temperature, then the zone fan was turned on by the PID controller. Overshoot of the temperature, typical with PID control, caused the fan to turn on often. The temperature of one zone interacts with the adjacent zone, therefore any temperature overshoot propagates along the extruder.

The ADRC algorithm was installed in programmable logic control code in parallel with the existing PID algorithm during a shift changeover. Overshoot and undershoot of zone temperatures that occurred with the original PID controls stopped within 15 minutes after the switch to the ADRC algorithm [19]. Temperature control of the extruder zones resulted in up to 58 percent reduction in power consumption of one of the production

lines. The utilization of ADRC in the polymer extrusion industry can be extended to use in control of other polymer variables.

2.4 Literature Review Summary

To summarize, the first-principle description of the dynamics of the polymer viscosity along the extruder length is complex for the case of plasticating extrusion, and increases in complexity for REX. This calls for regulation of viscosity using a method that follows a general approach, not requiring an accurate model of the transient behavior for the specific polymer, grade and process. This method must also incorporate a method for regulation of viscosity in the presence of any disturbances or changes in the dynamics.

Research in polymer extrusion viscosity regulation has focused on algorithms of the PI and PID such as MV, STR, Smith Predictor, and fuzzy scheduled. Any change in material or operating conditions requires a change to the parameters, or gains, of these forms of PID control. A better method for regulation of viscosity is one in which an estimated model of the process, which can be used for several polymer material grades, may be utilized. The method of ADRC is an excellent candidate for viscosity regulation. The change in materials, operating conditions, and output disturbances are all grouped together as general disturbance in the ADRC method. With ADRC, an accurate model of the process is not needed, and the general disturbance is tracked and cancelled in the control law.

CHAPTER III

VISCOSITY PROBLEM DESCRIPTION AND REFORMULATION

The mathematical description of solid bed and dynamic temperature profiles used to understand the transient behavior of viscosity is stated Section 3.1. The mathematical description is based on conservation of mass and energy equations. The problem description of viscosity regulation is given in Section 3.2. The plant model for viscosity regulation of extruded low density polyethylene (LDPE) for a given extruder at specific operating conditions is given in Section 3.3. The control law in the form of PID and ADRC are given in Sections 3.4 and 3.5, respectively.

3.1 Mathematical Description

The complexity of the transient behavior of viscosity in polymer extrusion can be understood by looking at the mathematical equations that describe the solid bed and dynamic temperature profiles in polymer extrusion, published by Zehev Tadmor [23]. The first equation is based on a mass balance for calculating the instantaneous solid bed profile (SBP). The second equation is based on an energy balance for calculating the instantaneous dynamic temperature of the melt pool.

The solid bed denotes the amount of material that has not melted inside the area surrounded by the extruder barrel and the screw channel. The width of the solid bed in the cross-section of the screw channel is a function of down channel distance, the path of which is the helical path of the screw channel. As the polymer travels along the extruder axial direction in the melting zone, the solid bed width within the helical screw channel decreases and the melt pool size increases.

The first equation of the SBP [23] is:

$$-\rho_s V_{sz} \frac{\partial(HX)}{\partial z} - \phi X^{1/2} = \rho_s \frac{\partial(HX)}{\partial t} \tag{3.1}$$

where ρ_s is the bulk density of the solid bed, *X(z, t)* is the width of the solid bed at position *z* and time *t*, $V_{sz}(t)$ is the down channel velocity of the solid bed, *H(z)* is the channel depth and the product $\phi(z,t)X^{1/2}$ is the rate of melting per unit down channel length. The variable *z* is the coordinate axis that follows the helical path of the polymer melt as it travel along the channel of the screw. The variable ϕ is a function of the operating conditions and the physical properties which affect the rate of melting. These

variables include barrel temperature, T_b, flow rate, Q, screw speed, w, viscosity, μ, thermal conductivity of the melt, heat of fusion and specific heat of the solid. The first three variables can be manipulation variables or are otherwise considered to be load variables. The other variables are properties of the polymer that change along the length of the extruder during the process and are typically not known. A schematic of these variables is shown in Figure 3.1 along with variables that will be defined in this section.

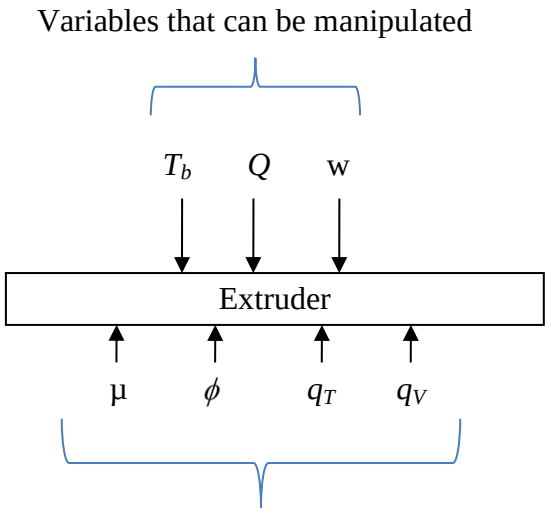

Figure 3.1 Characteristic of extruder variables.

The first and second terms of the left side of Equation 3.1 are the net rate of mass flow and the rate of melting respectively. The right side of the equation is the rate of mass accumulation.

Equation 3.1 can be rearranged, with A denoting the taper of the channel:

$$\frac{DX}{Dt} = \frac{\partial X}{\partial t} + V_{sz}\frac{\partial X}{\partial z} = -\frac{\phi}{\rho_s H}X^{1/2} + A\frac{V_{sz}X}{H} \tag{3.2}$$

$$A = -\frac{dH}{dz} \tag{3.3}$$

Equation 3.2 describes the change in the solid bed width with time in a coordinate system that moves at velocity $V_{sz}(t)$. This equation can be integrated if $\phi(z,t)$ is known. If $\phi(z,t)$ is replaced with ϕ_c, a constant, and if A is set to 0, then integration of Equation 3.2 for an initial profile of $X(z,t_0) = X_0(z)$, the SBP at time t is described:

$$X(z,t) = \hat{X}_o(z,t)\left[1 - \frac{(t-t_o)\phi_c}{2\rho_s H\sqrt{X_o(z,t)}}\right]^2 \tag{3.4}$$

where

$$\hat{X}_o(z,t) = X_o\left[z - (t-t_o)V_{sz}\right] \tag{3.5}$$

The width of the solid bed at a position z, and time t, is a function of the width at some previous time t_o and upstream at position $z_o(t)$:

$$z_o(t) = \left[z - (t-t_o)V_{sz}\right] \geq 0 \tag{3.6}$$

which is not smaller than the point where melting starts. The transient time is proportional to down channel location:

$$t - t_o = \frac{z}{V_{sz}} \tag{3.7}$$

In the case of constant flow rate the longest transient is equal to the residence time of the process. Substituting the longest transient time as calculated with Equation 3.7 into Equation 3.4 yields the steady-state profile:

$$X(z) = X_o(0)\left(1 - \frac{z\phi_c}{2V_{sz}\rho_s H\sqrt{X_o(0)}}\right)^2 \tag{3.8}$$

The differential energy balance of the melt pool in the polymer extrusion process explains the melt temperature profile, which is the variation in melt temperature along the helical screw channel:

$$\rho_m C_m \frac{\partial}{\partial t}\left[H(W-X)(T-T_r)\right] + C_m \frac{\partial}{\partial z}\left[G_m(T-T_r)\right]$$

$$= C_m \phi X^{1/2}(T_f - T_r) + q_T + q_v \tag{3.9}$$

where ρ_m and C_m are the density and specific heat of the melt respectively, W is the channel width, T_r and T_f are respectively reference and film temperatures and G_m is the mass flow rate of the melt. The left side of (3.9) is the sum of the accumulation of heat in the melt and the net convection of heat in the direction of flow. The right side of (3.9) is the heat convection from the melt film plus the net heat transfer through the walls, denoted by q_T, plus the heat generated by viscous dissipation, denoted by q_v. In order to solve (3.9), $G_m(z, t)$, $q_T(z, t)$ and $q_v(z, t)$ must be available. The derivative of the melt temperature is mathematically described in (3.11), derived from substitution of the equation of the mass balance of the melt (3.10) into (3.9), with q_T and q_v evaluated on instantaneous local conditions:

$$\frac{\partial G_m}{\partial z} = \phi X^{1/2} + \rho_m \frac{\partial(XH)}{\partial t} \tag{3.10}$$

$$\frac{DT}{Dt} = \frac{\partial T}{\partial t} + V_{mz}\frac{\partial T}{\partial z} = \frac{\phi X^{1/2}(T_f - T)}{\rho_m H(W-X)} + \frac{q_v + q_T}{G_m C_m H(W-X)} \tag{3.11}$$

where V_{mz} is the mean melt velocity and $(W\text{-}X)$ is the width of the melt pool:

$$V_{mz} = \frac{G_m}{\rho_m H(W - X)} \tag{3.12}$$

Further analysis of Equation 3.11 is difficult due to the complex dependence on time through *X*. Also, the variables q_T and q_v are functions of the local temperature. Integrating (3.11) numerically, and given an initial temperature profile $T(z, t_o)$ and the melt temperature at the inlet of the melting zone $T(z_o, t)$ as boundary conditions, the temperature profile $T(z, t)$ at all future time t greater than t_o can be calculated provided that the SBP, G_m, q_v and q_T are known. A total mass balance can be obtained by adding the mass balance on the solid (3.1) to the mass balance on the melt (3.10) which leads to:

$$\frac{\partial G}{\partial z} = \frac{\partial G_m}{\partial z} + V_{sz}\rho_s \frac{\partial(XH)}{\partial z} = (\rho_m - \rho_s)\frac{\partial(XH)}{\partial t} \tag{3.13}$$

Equation 3.13 describes the total change in mass flow along the helical screw channel. In this equation, the net accumulation through convection is equal to the net accumulation due to change in average density. If the melt density is assumed to be equal to the solid density, which is a reasonable assumption, then (3.13) is simplified to:

$$G_m = G - V_{sz}\rho_s XH \tag{3.14}$$

The complexity of the equations require recursive integrations of the differential mass balance on the solid bed (3.2) and the differential energy balance on the melt pool (3.11) with initial conditions of *X* and *T* if they are to be implemented in a controller. The connection between the mass and energy balance equations and viscosity control is through (3.14) and the following equation which describes the flow rate-pressure drop relationship at the die:

$$G = K_{DIE}\rho_m \frac{\Delta P_D}{\mu_D} \tag{3.15}$$

where K_{DIE} is a constant depending on the die geometry, μ_D is the mean viscosity at the die, and ΔP_D is the pressure drop across the die. The recursions of the integrations are complete when the initial guess of a variable in (3.15), such as ΔP_D, is satisfied by a convergence of G in equations (3.15) and (3.14).

It is not realistic to use the recursive integrations in an industrial application of viscosity control. The complexity of the equations that describe the dynamics of polymer extrusion and the variations in extrusion operating conditions and properties of the polymer ingredients call for a controller algorithm that can accommodate unknown dynamics and reject variable disturbances.

3.2 Problem Description

Yang and Lee [6] present a list and discussion of possible load, manipulation, and control variables in polymer extrusion. A manipulated variable is a variable that can be changed by external manipulation. A control variable is controlled through the manipulation variable. A load variable is any variable that may present disturbance to the control variable or manipulation variable.

The consideration of a parameter as a load variable depends on the selection of control and manipulation variables. For example, barrel temperature, die pressure, and resin properties are load variables in a process in which extrudate quality is a control

variable and screw speed is a manipulation variable. A change in any of these variables could be considered a disturbance, and would have an effect on the viscosity.

Figure 3.2 shows the block diagram representation of a feedback viscosity control loop in which screw speed is the manipulation variable. The plant is a term for the process to be controlled, in this case the extrusion process. The variable *e* represents the error, or difference between the set-point and the output. The output viscosity is subtracted from the set-point viscosity, and the error is fed into the controller. The controller manipulates the control signal, shown as *u* in the diagram, and sends the control signal to the plant. The load variables in Figure 3.2 are barrel temperatures (T_b), die pressure (P), and feed properties. Key in viscosity control is disturbance rejection.

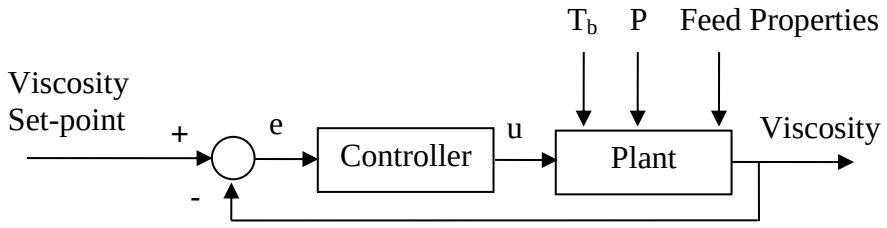

Figure 3.2 Block diagram of viscosity control.

3.3 Plant Model

Chiu and Pong [11] studied viscosity control of an unspecified grade of low density polyethylene (LDPE) with screw speed as the manipulation variable. A second order

model was developed empirically by Chiu and Pong through step response tests. Their data from a given operating range was fit to this second order model expressed in the continuous-time Laplace domain, of the form found in any controls textbook [35]:

$$Y(s) = \frac{K\omega_n^2}{s^2 + 2\xi\omega_n s + \omega_n^2} U(s) \tag{3.16}$$

where $Y(s)$ is the output, in this case viscosity with the units of Pascal-seconds (Pa-s); $U(s)$ is the input, in this case screw speed with the units revolutions per minute (rpm); K is the process gain; ξ is the damping ratio; and ω_n is the natural frequency. At a specific operating range, Chiu and Pong fit the plant step response data to this second order model with values stated in their paper of K= -928.488 Pa-s per rpm, ξ = 0.53, and ω_n = 2.54 radians per second. Inserting these values into (3.16), and transforming the equation into the time domain, the equation is in the form of a linear time-invariant second-order plant:

$$\ddot{y} = -2.6924\dot{y} - 6.4516y - 5990.23u \tag{3.17}$$

Equation (3.17) is used for the plant model in all simulations in this paper, with the addition of 35000 Pa-s to the viscosity, *y*, after the final integrator of the plant block model. This addition was made in order to obtain a viscosity response similar to the response stated in [11] for the open loop test of the extruder, which is represented in Figure 3.3. The step input block specifies the change in the screw speed, and the output of the plant model in Figure 3.2 is the viscosity. Figure 3.3 shows a white noise added to the output after the plant block. This white noise is zero in the simulation of the open

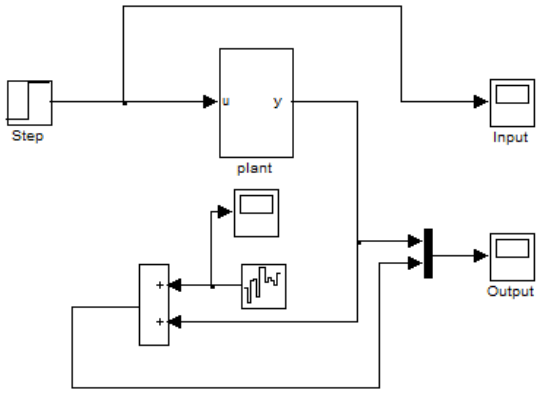

Figure 3.3 Simulink model of the open loop test for a plant response of viscosity to a change in screw speed.

loop test. An input step change from 10 revolutions per minute to 20 revolutions per minute at time equal to eight seconds is shown in Figure 3.3. The viscosity response to this input screw speed change is shown in Figure 3.4. This graph looks equivalent to the system response of the plant shown in [11].

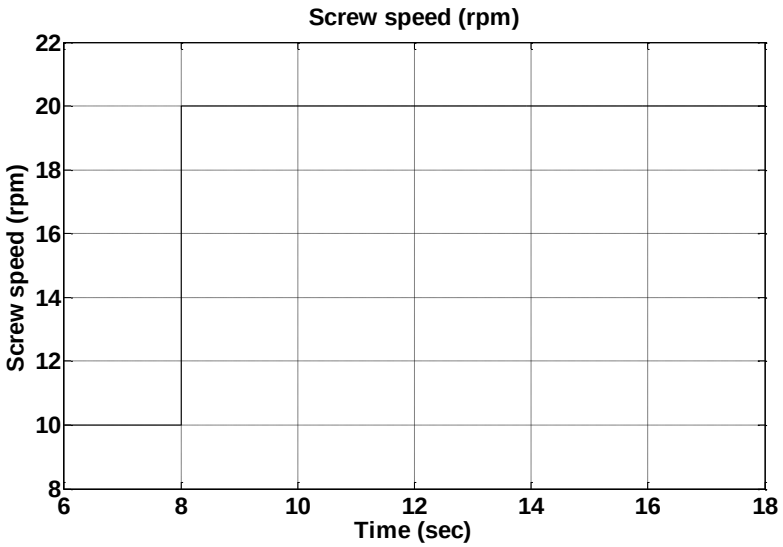

Figure 3.4 A step change in screw speed from 10 rpm to 20 rpm at *t* equals eight seconds in the Simulink model shown in Figure 3.2.

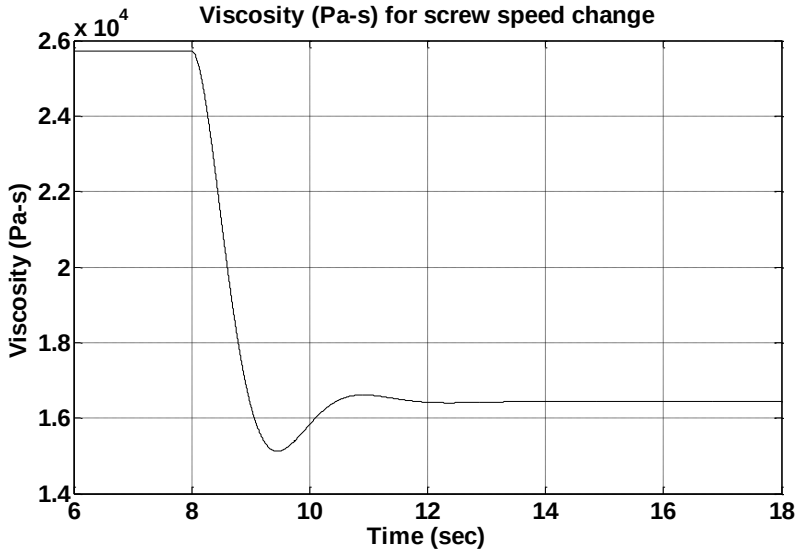

Figure 3.5 The viscosity response, with units of 10^4 Pa-s, to the screw speed change shown in Figure 3.3.

3.4 Control Law in the Form of PID

The most prevalent form of control in industry is PID control. It is typically tuned through trial and error. The traditional PID controller is defined by:

$$u = K_D\dot{e} + K_P e + K_I \int e \tag{3.18}$$

where K_D, K_P *and* K_I are controller parameters, also known as gains, of the PID to be selected. In (3.18), u is the control signal or control law and e is the error, which are shown in Figure 3.2; $\dot{e}$ represents the error trend, and $\int e$ represents the accumulated error. The tuned gains of the PID used in viscosity control can be thrown off by slight disturbances to the system.

3.5 Control Law in the Form of ADRC

Consider the second-order plant in (3.17), with disturbances written in the form:

$$\ddot{y} = f\left(y, \dot{y}, d, t\right) + bu \tag{3.19}$$

where y is the output, u is the control signal or control law, b is a constant, and d represents disturbances. In the active disturbance rejection control (ADRC) framework, the entire $f\left(y, \dot{y}, d, t\right)$ is assumed unknown and is denoted as the generalized disturbance. It includes not only the disturbances but the internal dynamics of the system. If f from (3.19) can be estimated as $\hat{f}$, then the control law:

$$u = \frac{\left(-\hat{f} + u_0\right)}{b_0} \tag{3.20}$$

reduces the plant to:

$$\ddot{y} \approx u_0 \tag{3.21}$$

where:

$$u_0 = k_p\left(r - z_1\right) + k_d z_2 \tag{3.22}$$

which transforms a nonlinear, unknown, and time-varying plant to an easy to control plant. In (3.22) the variables k_p and k_d are the parameterized gains in the ADRC controller based on the controller bandwidth, ω_c [34]:

$$k_p = \omega_c^2 \tag{3.23}$$

$$k_d = 2\omega_c \tag{3.24}$$

The values of z_1 and z_2 of (3.22) come from the unique state observer known as the Extended State Observer (ESO) [34]. The value of $\hat{f}$ also comes from the ESO. To understand how this disturbance is estimated by the ESO, consider (3.19) in the form of a linear time-invariant second-order plant:

$$\ddot{y} = -a_1\dot{y} - a_0 y + bu \tag{3.25}$$

with a_0 and a_1 unknown, and $f = -a_1\dot{y} - a_0 y$ in this particular case. The ADRC framework estimates f even as a_0 and a_1 vary. The state space model of (3.25) is changed to include an additional state f. Let $x_1 = y$, $x_2 = \dot{y}$, and $x_3 = f$. Assuming f is differentiable, let $h = \dot{f}$. The revised model of (3.25) is:

$$\begin{cases} \dot{x} = Ax + Bu + Eh \\ y = Cx \end{cases} \tag{3.26}$$

where:

$$A = \begin{bmatrix} 0 & 1 & 0 \\ 0 & 0 & 1 \\ 0 & 0 & 0 \end{bmatrix}, B = \begin{bmatrix} 0 \\ b_0 \\ 0 \end{bmatrix}, E = \begin{bmatrix} 0 \\ 0 \\ 1 \end{bmatrix},$$

and $C = \begin{bmatrix} 1 & 0 & 0 \end{bmatrix}$. The ESO is a state observer of (3.26):

$$\begin{cases} \dot{z} = Az + Bu + L(x - z) \\ \hat{y} = Cz \end{cases} \tag{3.27}$$

where $L = \begin{bmatrix} l_1 & l_2 & l_3 \end{bmatrix}$ is the observer vector gain which is chosen so that all the observer eigenvalues are located at $-\omega_o$ [23] for the characteristic equation:

$$\lambda^3 + l_1\lambda^2 + l_2\lambda + l_3 = (\lambda + \omega_0)^3 \tag{3.28}$$

The value of ω_o is the observer bandwidth. With a well-tuned observer, z_1, z_2, and z_3 closely track y, $\dot{y}$, and f, respectively.

With the ADRC framework, the first two terms on the right side of (3.17) are treated as the equation of *f*. Equation (3.17) becomes:

$$\ddot{y} = f(y, \dot{y}, d, t) - 5990.23u \tag{3.29}$$

in which an estimate of the coefficient of *u* is needed, but it does not have to be accurate. The system is then reduced to a simple double-integral plant with a scaling factor b_0. Notably, the nonlinear characteristic of viscosity control in polymer extrusion can be handled with ADRC.

CHAPTER IV

SIMULATION VALIDATION

Simulations of PI control and ADRC were performed for comparison. The simulations represent closed-loop control of the same plant. The plant used in the simulations is (3.17), described in Section 3.3. A change in dynamics of the plant are considered in Section 4.1, and used for the PI simulations comparison in Section 4.1 and in the final simulation of ADRC in Section 4.2.

In all simulations, a step set-point change from 25,500 Pa-s to 16,000 Pa-s is set at time equal to 40 seconds. A sampling time of 0.01 second was used. At time equal to 80 seconds, a step disturbance of 1600 Pa-s is added. This disturbance is added to simulate a change in grade of the polymer being introduced to the extruder at the feed-throat. The change in grade was approximated with a 0.5 second time constant, which is reasonable as seen in disturbance simulations in [13]. In industry, viscosity control does not typically involve a step set-point change in the reference signal of the closed-loop control of viscosity, but instead, a constant reference signal. Therefore, the viscosity is controlled to

a constant set-point of 16,000 Pa-s in these simulations. The focus of this section is on the response to the disturbance added at time equal to 80 seconds.

4.1 PI Simulation

The Simulink model of closed-loop control with the PI controller is shown in Figure 4.1. A white noise power level of 10 is first used in two simulations of the PI controller to simulate sensor noise, and then increased to 100 to verify that the PI can accommodate the higher level of noise for reducing error and bringing the process back to set-point. This higher level of noise is reasonable compared to the extruder sensor viscosity outputs shown in [11]. At the higher power level, it was determined that a derivative gain of a PID controller cannot be used because of its undesirable action upon the fast changing error that is seen by the controller. Therefore, only the proportional and integral gains of the controller were used in these simulations. The white noise power level of 10 is used for the first figure in this section to make it easier to see and compare the characteristics of the viscosity error and the control law of the PI controller for two PI simulations. The final figure in this section has a noise power level setting of 100.

Two simulations of the PI controller were completed to show that a change in plant dynamics of a system controlled with the same traditionally tuned PI controller will have different viscosity and control law responses for viscosity control. The traditional PI will act upon the error and reduce it, but may have higher oscillation amplitude to bring the process to set-point if the system dynamics or the disturbances are different from those

for which the PI was tuned. The PI controller for the plant of (3.17) for a step disturbance previously described was tuned through trial and error using the plant model in Figure 3.3. Since common industry practice is to maintain a viscosity equal to a constant reference signal, the PI in this simulation is tuned to maintain a constant set-point for the desired response to a maximum 10 percent step disturbance in viscosity, simulated as a change in polymer property.

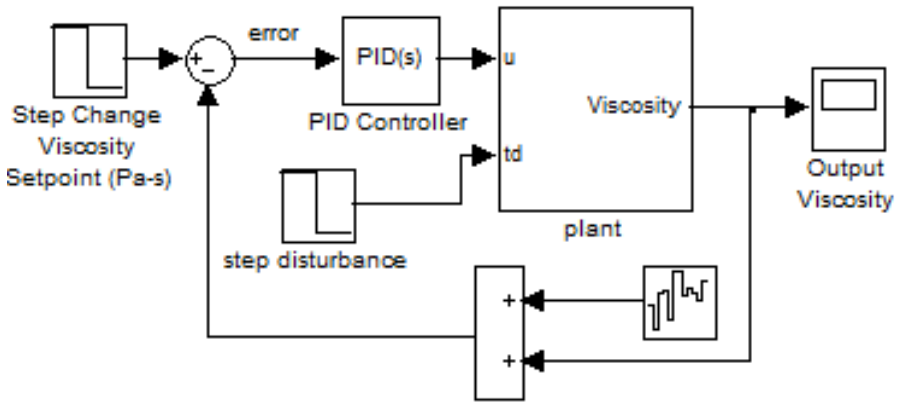

Figure 4.1 Simulink model of the plant with a PI controller.

Traditional PID tuning is based on trial and error. It is common practice to start at a proportional gain, K_P, with a small derivative gain, K_D, to cause the output of the closed-loop system to oscillate without damping. For this reason, the K_D value was included initially in the tuning process and then removed, while using a very small noise power level of (1e-9) in the Simulink model. Initially a value of -0.3 for K_P and -0.03 for K_D and

-2.8 for the integral gain, K_I, were used. The process of tuning the PID involves an iterative procedure of adjusting all three gains so that the oscillation of the manipulated variable is centered about the mean of the control signal, and the oscillation of the controlled variable is decreased. The former is achieved with iterative changes in all three variables; the latter is achieved with decreases in K_P, along with slight increases in K_D and slight decreases in K_I.

This tuning procedure from my starting point for the three gains turned out to be a very long process. After bringing the values of K_P, K_I, and K_D down to -0.2, -0.3, and -0.05 respectively, all three variables eventually had to be divided by approximately 100. A smooth response with no oscillation of viscosity error and only a small oscillation of control law was achieved with the final PID gains tuned to K_P =-0.002247, K_I =-0.003666, K_D =-0.000341. The derivative gain was then removed. A PI rather than a PID is chosen due to the high sensor noise level commonly seen in polymer extrusion [11, 13].

After the PI gains were put into the Simulink plant model, a change was made to the plant's natural frequency and the process gain. The process gain was changed to simulate the nonlinearity of viscosity in relationship with shear rate, which is a function of the screw speed. The change in natural frequency was made to the plant to simulate a change in the internal dynamics of the plant. The combination of the changes in natural frequency and process gain can also be treated as an inaccurately modeled plant. The natural frequency was reduced to 80 percent of the natural frequency of (3.17), so that the new natural frequency, ω_n, is 2.0329. The process gain of the plant, K, was decreased in magnitude from -928 to -800. The new plant equation, which consists of a reduction in

magnitude of the process gain and a twenty percent decrease in natural frequency of (3.17):

$$\ddot{y} = -2.15488\dot{y} - 4.1327y - 3306.16u \tag{4.1}$$

The plant block of Figure 4.1 was changed to reflect this new equation (4.1), and a second simulation, this time of the closed-loop response of the plant of Figure 4.1, was completed with the same PI tuned above, and a noise power level of 10. Figure 4.2 compares the viscosity error and screw speed for both simulations with the same PI controller. This shows that a small change in the dynamics or an inaccurate model of the extrusion process can have an increase in initial error and amount of oscillation of the output for the same PI controller. Simulation results for a noise power level of 100 are shown in Figure 4.3.

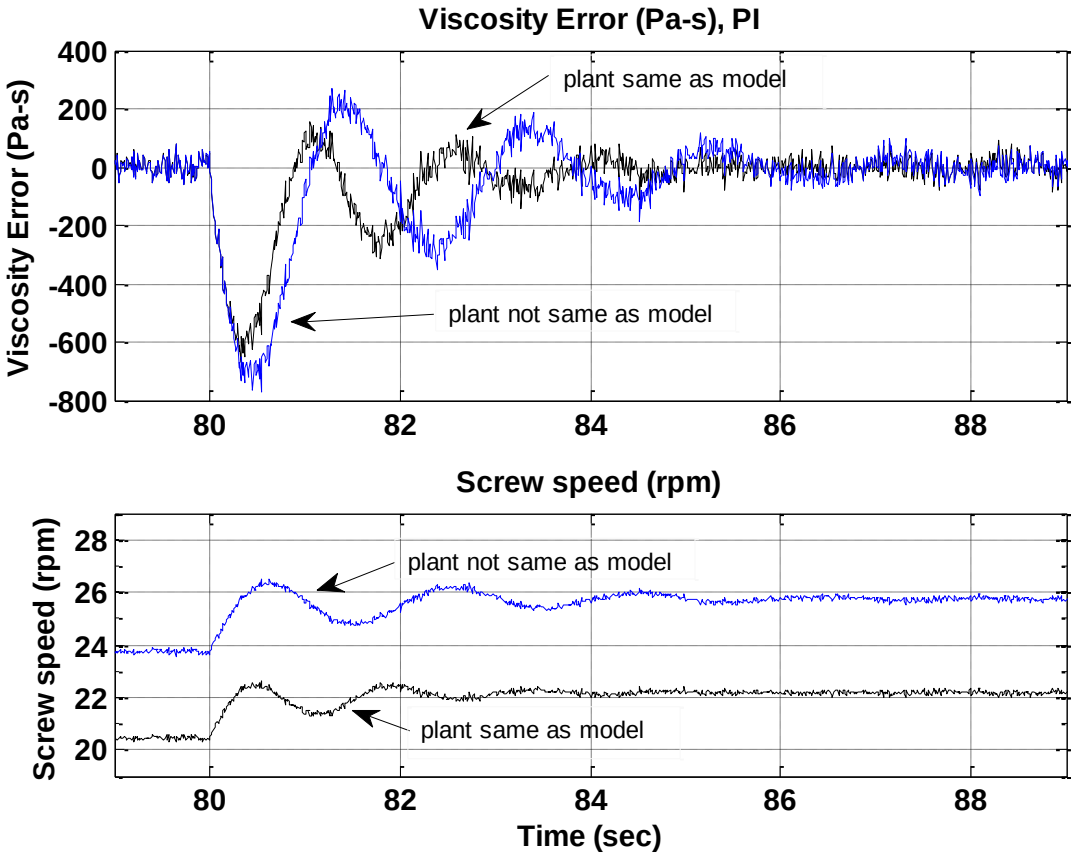

Figure 4.2 Viscosity error and screw speed each versus time with noise power level of 10, for systems (3.17) and (4.1) each with the same PI controller gains of K_P =-0.002247 and K_I =-0.003666. Each system has a step disturbance of 1600 Pa-s added at t=80 seconds.

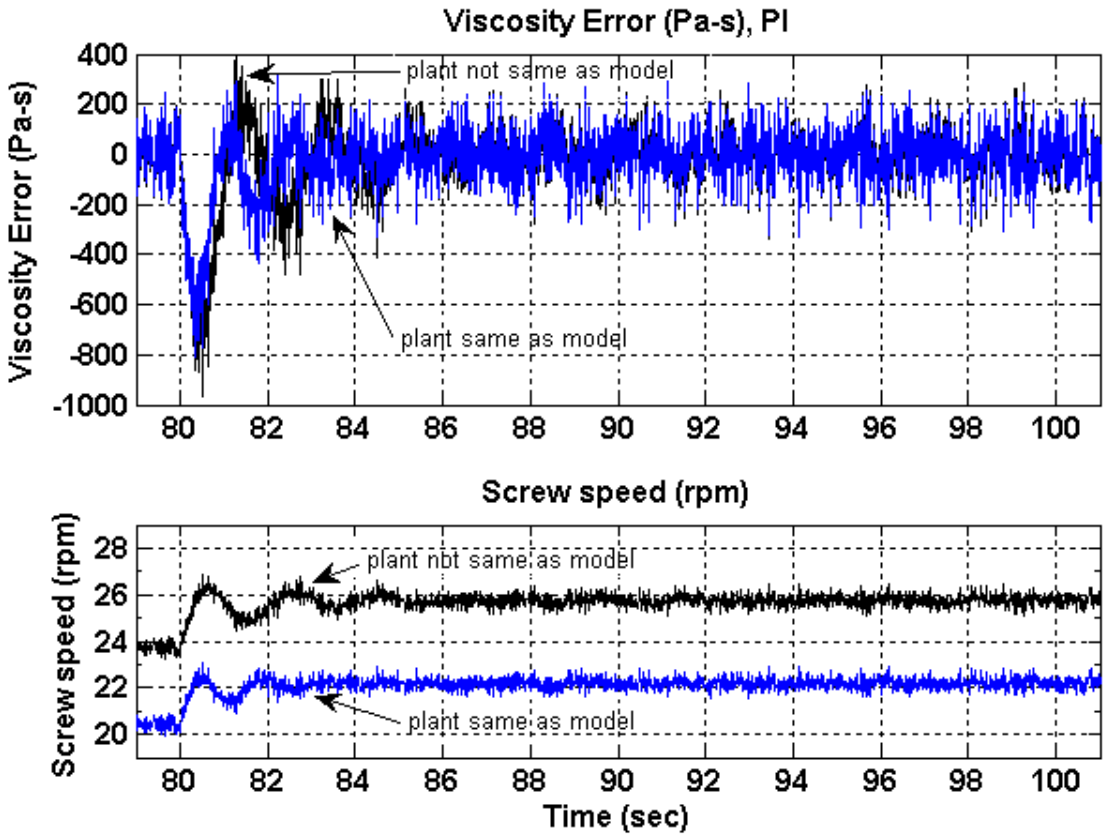

Figure 4.3 Viscosity error and screw speed each versus time with noise power level of 100, for systems (3.17) and (4.1) each with the same PI controller gains of K_P =-0.002247 and K_I =-0.003666. Each system has a step disturbance of 1600 Pa-s added at t=80 seconds.

4.2 ADRC Simulation

Two ADRC simulations with b_0 values of -5990 and -9000 were completed for the same plant (3.17) with the model shown in Figure 4.4. The large block in Figure 4.4

includes the ADRC framework with the plant. The parameters needed for tuning the observer and controller in the ADRC framework are b_0; the observer bandwidth, ω_o, mentioned in the Section 3.4, and the controller bandwidth, ω_c. The values of *kp* and *kd* shown in Figure 4.4 are functions of the controller bandwidth, ω_c. The value of *kp* in this simulation is set to twice the negative value of ω_c, which is added to the error before the division by *b0* in the Simulink model in Figure 4.4. Before the simulations, the bandwidths of the controller and observer were tuned, and chosen to be 9.0 radians per second for ω_c and 3.0 radians per second for ω_o.

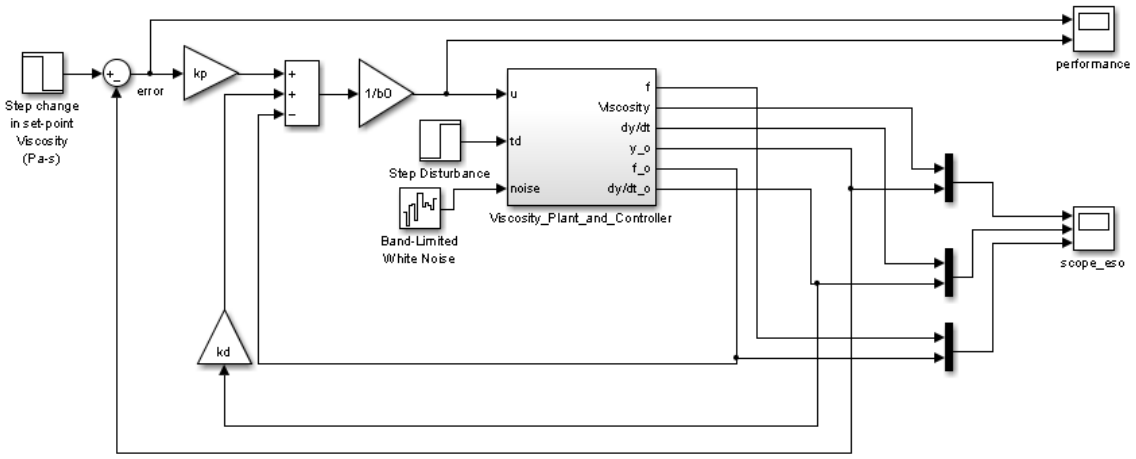

Figure 4.4 Simulink model of the plant with the ADRC observer and controller.

The same step disturbance of 1600 Pa-s that was added in the PI simulation at time equal to 80 seconds is included in both ADRC simulations of the model (3.17) shown in Figure 4.4. A band-limited white noise power level setting of 100 was included in the ADRC simulation to represent an actual sensor noise, in order to verify the satisfactory control of

ADRC with the chosen values of ω_c and ω_o. The noise power level was then decreased to 10 so that a clear observation may be made of how closely the observer tracks *y*, *dy/dt*, and *f*. Viscosity is represented by the variable *y*. The noise power level waws kept at 10 for the plot of two different simulations with two different b_0 values on the same graph. The b_0 value in the first simulation is -5990 and the b_0 value in the second simulation is -9000. The results of the first and second simulations are shown in Figure 4.5 and Figure 4.6, respectively. The observer values, shown in blue, follow the viscosity closely and trail behind the actual values in the graphs of *dy/dt* and *f*.

The plot of the viscosity error and the plot of the control signal, comparing both values of b_0, are given in Figure 4.7. This figure shows a maximum viscosity error of approximately 500 Pa-s for b_0 set to -5990 and -9000 for the ADRC simulations. The control law in both ADRC simulations has a smoother signal to the screw motor than the control signal of the PI controller, as seen in comparison of Figure 4.7 with Figure 4.2. The large amplitude oscillation is shorter in length of time in ADRC than for the PI controller.

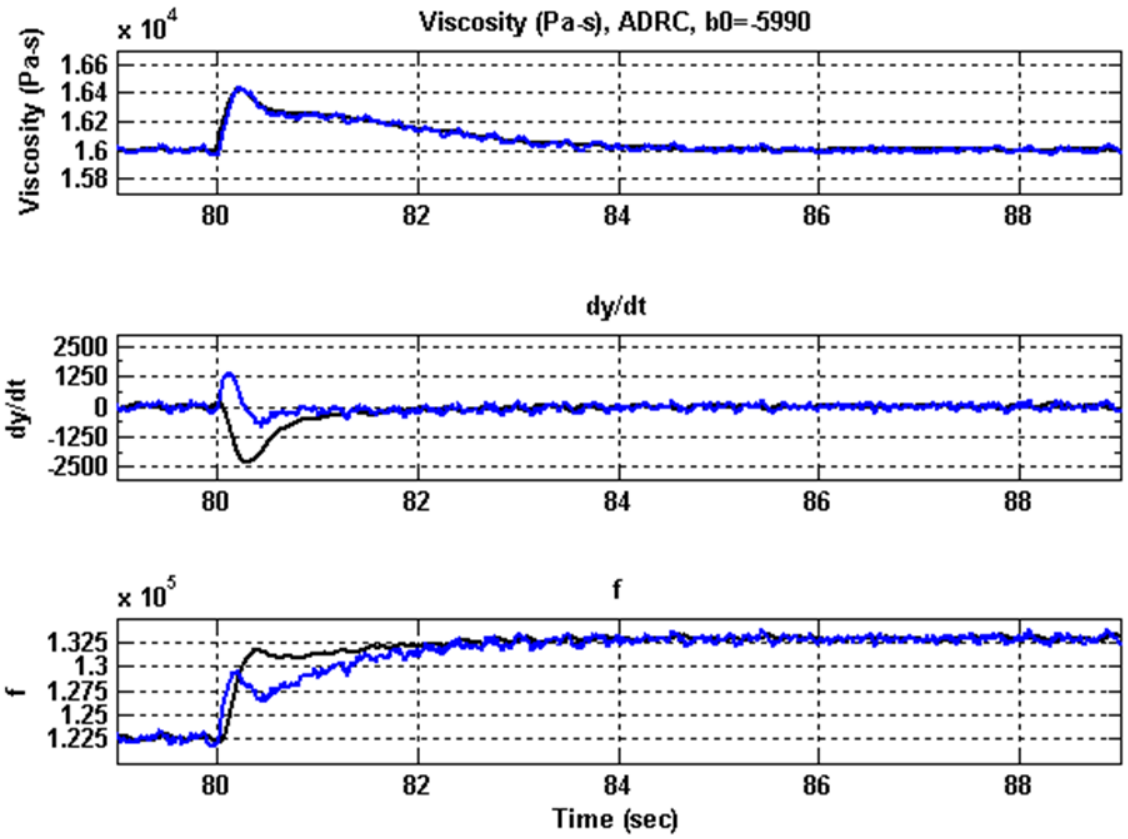

Figure 4.5 Actual and observer-tracked viscosity, *dy/dt*, and *f* plots versus time with ADRC for b_0=-5990, with 1600 Pa-s disturbance added at *t*=80 seconds to the plant (3.17) with noise power level setting of 10.

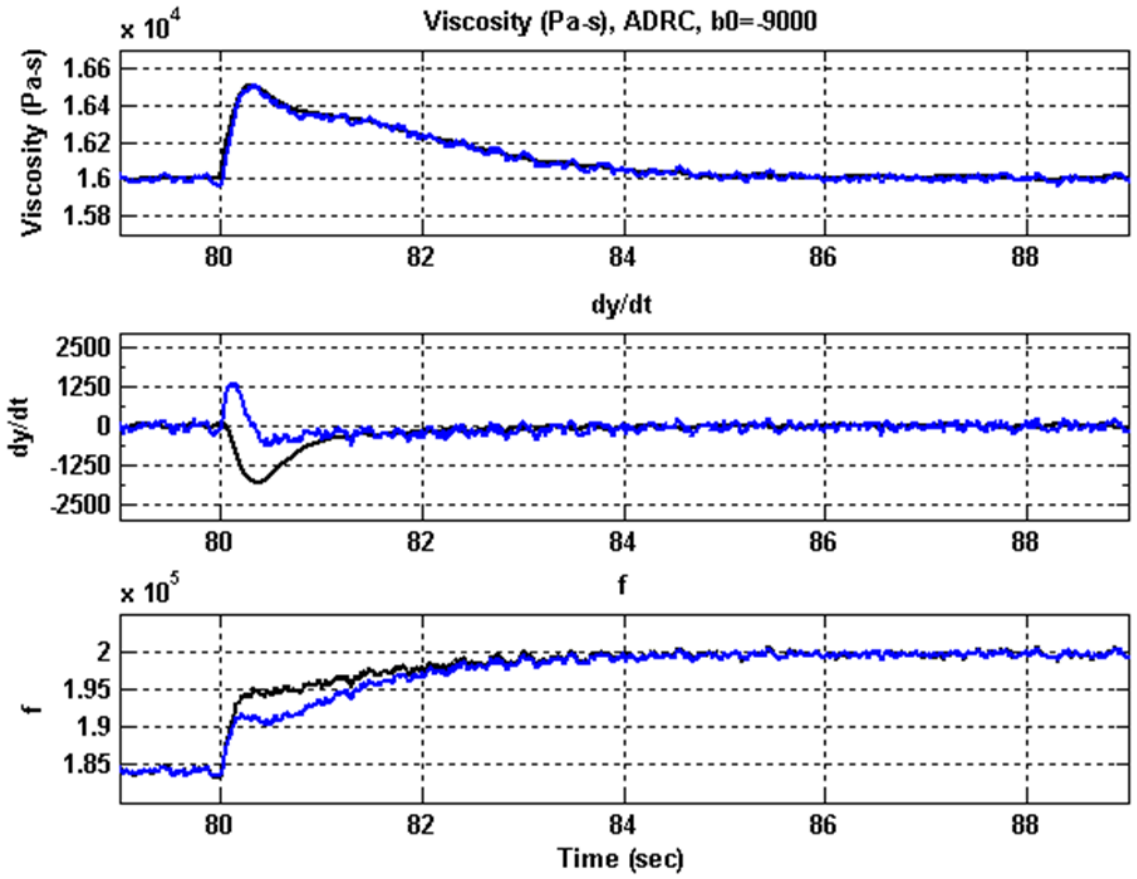

Figure 4.6 Actual and observer-tracked viscosity, *dy/dt*, and *f* plots versus time, with ADRC for b_0=-9000, with 1600 Pa-s disturbance added at *t*=80 seconds to the plant (3.17) with noise power level setting of 10.

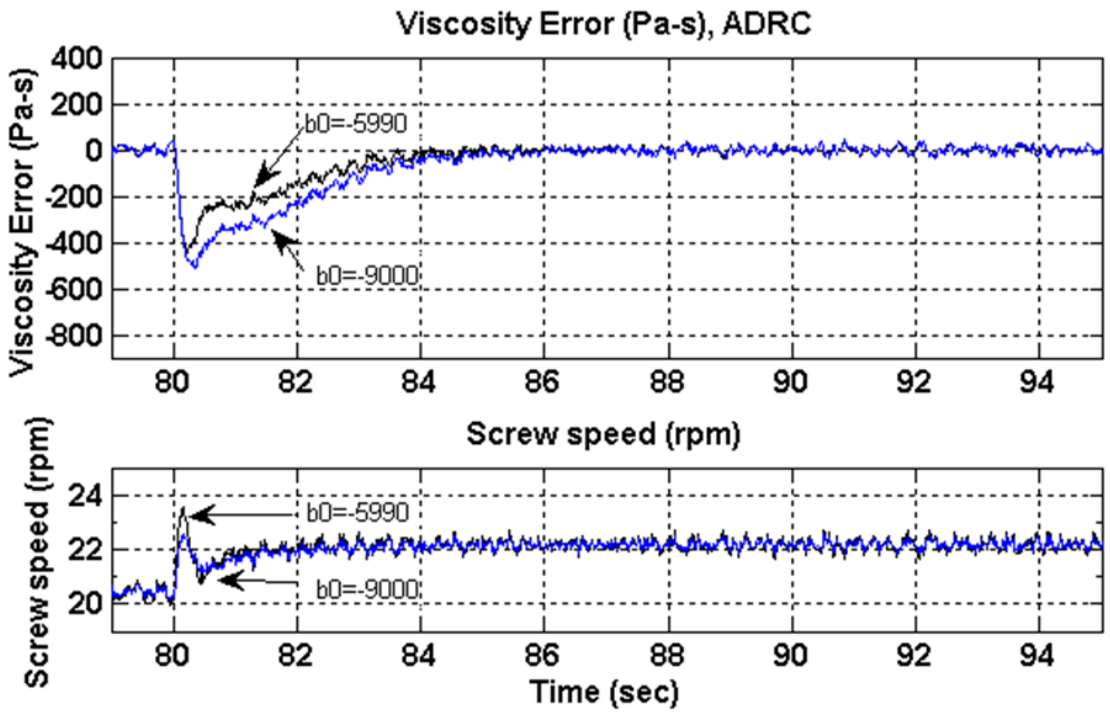

Figure 4.7 The viscosity error and the screw speed versus time, with ADRC control for b_0=-5990 and b_0=-9000, with 1600 Pa-s disturbance added at t=80 seconds to the plant (3.17) with noise power level setting of 10.

Finally, a simulation of ADRC with b_0 setting of -9000 for the inaccurately modeled plant (4.1) was completed and compared to the PI controller for the inaccurately modeled plant (4.1), for the same disturbance of 1600 Pa-s added at time equal to eighty seconds. Figure 4.8 and Figure 4.9 show comparisons of the ADRC and PI simulations with noise power level settings of 10 and 100, respectively. Less oscillation of the motor speed is evident in the ADRC simulation with b_0 setting of -9000 compared to the PI simulation. Figure 4.8 and Figure 4.9 show the viscosity settles to within 100 Pa-s of the set-point viscosity within three and a half seconds for ADRC, compared to five seconds

for the PI controller. A higher initial viscosity error is evident with the PI controller, as seen in Figure 4.8 and Figure 4.9. A faster settling time and smoother viscosity output and control signal were accomplished with ADRC. More importantly, ADRC accomplished satisfactory disturbance rejection and viscosity regulation of an inaccurately modeled plant.

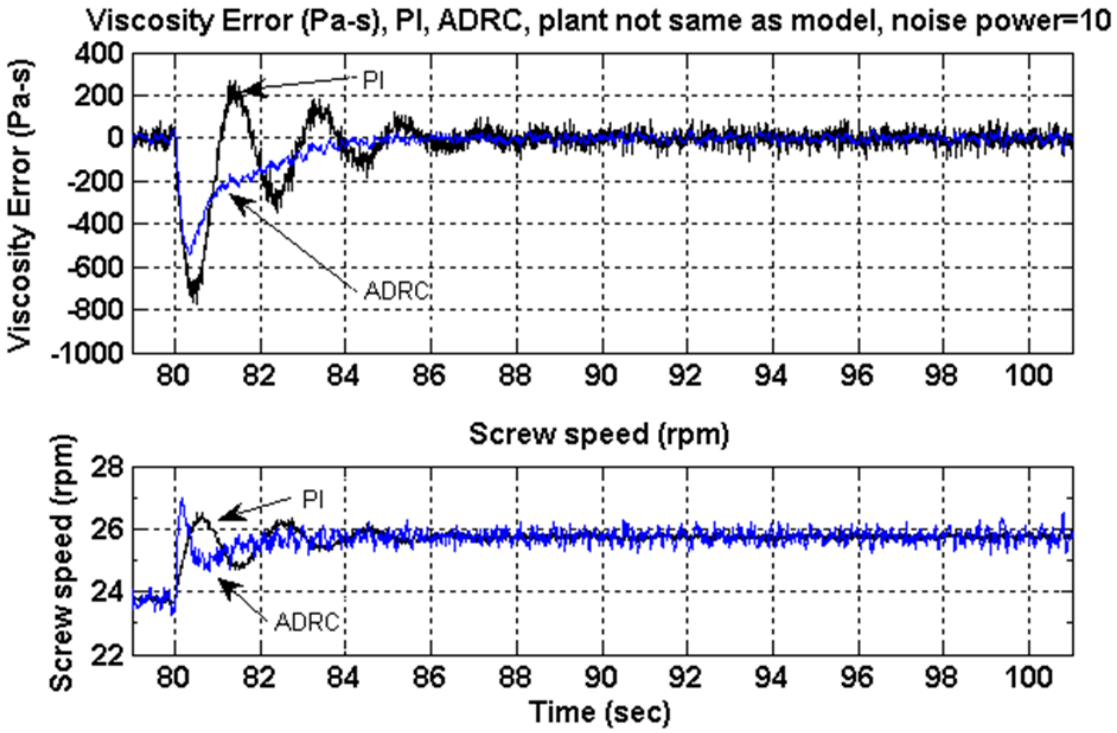

Figure 4.8 Comparison of the viscosity error and the screw speed versus time for PI and ADRC with b_0=-9000, for the inaccurately modeled plant (4.1) and 1600 Pa-s disturbance added at t=80 seconds, with noise power level setting of 10.

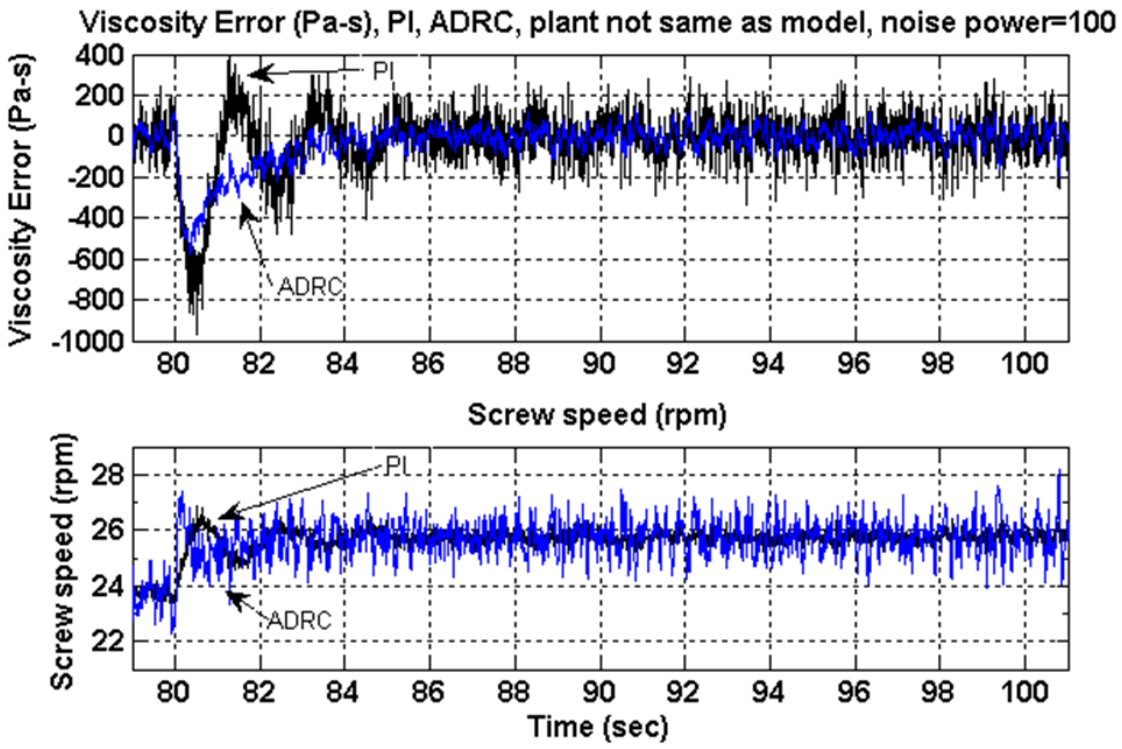

Figure 4.9 Comparison of the viscosity error and the screw speed versus time for PI and ADRC with b_0=-9000, for the inaccurately modeled plant (4.1) and 1600 Pa-s disturbance added at t=80 seconds, with noise power level setting of 100.

CHAPTER V

EXPERIMENTAL RESULTS

In this chapter, a circuit which is hardwired directly to an industrial controller, or to a personal computer that is loaded with Matlab, Simulink, and Windows Real-Time, simulates a plant of viscosity in extrusion. The modifications made to the circuit simulate a change in process gain and process dynamics. The circuit and its modifications are described in Section 5.1. The experimental set-up of the circuit with PI control is also described in Section 5.1. The results from the experiments of PI control in closed-loop with the original circuit and with the modified circuit are given in Section 5.2. The experimental set-up of the circuit with ADRC is described in Section 5.3. The results from the ADRC experiments and a comparison of these results with the results from the PI experiments are given in Section 5.4.

5.1 Experimental Set-up of PI Control

This section describes the design and set-up of an experiment of PI control of a circuit. The circuit simulates a plant that is equivalent to the plant used in the simulations of Chapter IV. Figure 5.1 shows a block diagram of the set-up used for the experiment of PI control of the circuit with an industrial controller. The circuit diagram includes a sub-circuit with a switch, which when closed, simulates the adding of a disturbance to the plant due to a property change in feed polymer.

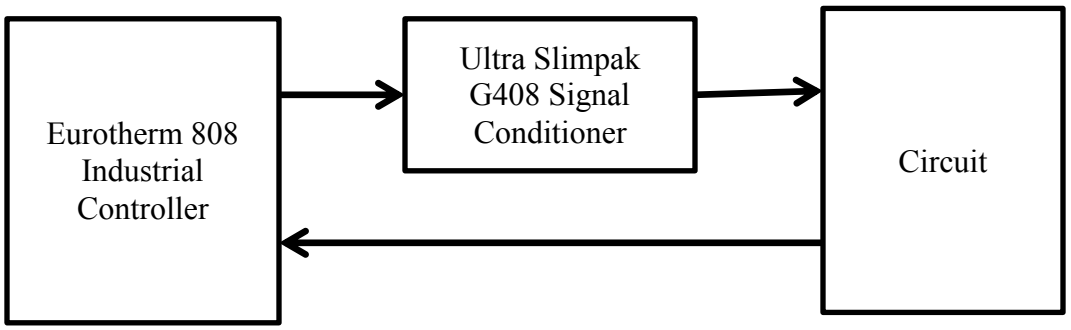

Figure 5.1 Block diagram of the set-up of the PI control experiment.

The first set of experiments with PI control is conducted at a sampling rate of eight hertz. The PI control at eight hertz is provided by a Eurotherm 808 industrial controller. A signal conditioner is necessary because the Eurotherm 808 controller is non-isolated between its input and its output electronics. The output of the Eurotherm controller is connected to the input of the signal conditioner, which provides signal isolation between

the Eurotherm 808 internal input and output electronic circuitry. The output of the Eurotherm controller is configured for a percent output of zero to twenty milli-amps. In other words, a value of 50.0 on the second line of the user screen corresponds to a 10.0 milli-amps current output from the controller for this configuration. The signal conditioner is configured for a zero to twenty milli-amps input and output.

The Eurotherm 808 controller can operate in manual or automatic mode. The change from manual to automatic mode is bumpless [36]. The operator display screen and buttons are shown in Figure 5.2. To switch from manual to automatic mode, or vice versa, the operator presses the A/M button. When in manual mode, an LED light is lit below the letter M, at the top of the display screen. Also, for the configuration of percent output that was set-up for this experiment, the percent output is shown in the bottom line of the display screen when the controller is in manual mode. When the controller is in automatic mode, the bottom line will show the set-point value. This set-point value may be increased or decreased while in automatic operation by pressing the up or down arrow, respectively. While in manual mode, the menu items may be chosen by pressing the PAR button. This allows parameters to be accessed. The arrow buttons are used to adjust the parameters.

For automatic and manual mode, the top line of the display is always the input measurement indication to the operator. The numeric value is determined by the configuration of the controller prior to operation. It is not typically the voltage or current numeric value, but rather a numeric number that has meaning to the operator. This numeric value is known as the process variable. The configuration of the process variable involves use of a voltage or current signal generator connected to the input terminals

Figure 5.2 Picture of user display and buttons of the Eurotherm 808 controller.

of the controller to set a numeric value to the applied signal. While in operation, the top line of the operator display will show the numeric value of the process variable. Also in the top line, a signal break or under range value is displayed as “Sn b” or “ur” respectively.

The terminals of the Eurotherm 808 are shown in Figure 5.3. The terminals at the top left corner of the photograph shown in Figure 5.3 are the output signal terminals. The output of the Eurotherm controller may be configured in the controller menu for zero to twenty milli-amps, four to twenty milli-amps, or zero to five volts. In this experimental set-up, the Eurotherm is configured for zero to twenty milli-amps. Terminals five, six and seven are the AC supply voltage lines. The right side of the photograph shown in Figure 5.3 displays two resistors connected to terminals 18, 19 and 20 with the wires for the controller input. The resistors and configuration in the controller menu are for a zero to ten volts input for this experiment. The two resistors are 220 ohms, connected to terminals 18 and 19, and 56 kilo-ohms, connected to terminals 19 and 20. This arrangement satisfies the equation: 40 milli-volts equals the maximum input voltage

times R_1, divided by the sum of R_1 and R_2, where R_1 is the 220 ohms resistor. For the set-up of these experiments, the maximum input voltage of the Eurotherm controller is configured for ten volts. The input signal may be configured in the controller menu as a current or a voltage signal. The other option for maximum input voltage is five volts. For an input current, an adapter is available with the necessary electronics, or one can be made with resistors.

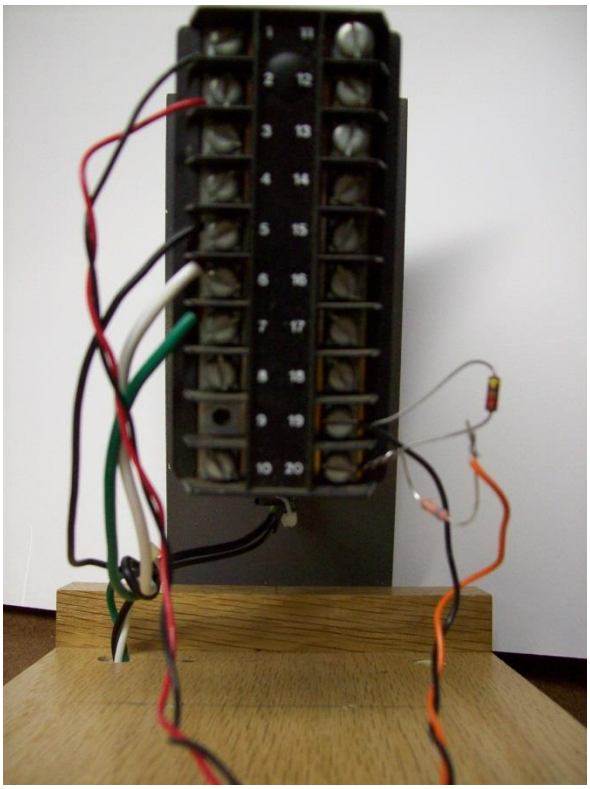

Figure 5.3 Picture of the terminals of the Eurotherm 808 controller.

The plant is contained in the circuit. The circuit diagram is shown in Figure 5.4. The output current from the signal conditioner is the input to a 250 ohms resistor sub-

circuit. The voltage across the 250 ohms resistor is multiplied by a designed gain of 18.1 by the top operational amplifier and resistor configuration in the diagram shown in Figure 5.4. The output of this operational amplifier is the input into a Sallen-Key architecture used to simulate the second-order behavior of the plant. The Sallen-Key architecture is composed of the bottom operational amplifier, two 8.2 kilo-ohms resistors, 100 micro-farads capacitor, and 22 micro-farads capacitor shown in the bottom of the diagram in Figure 5.4. The resistors and capacitors in the Sallen-Key architecture determine the natural frequency of the plant.

The sub-circuits SC1 and SC2 are shown in the diagrams in Figure 5.5 and Figure 5.6, respectively. The voltage across the one giga-ohm resistor at the bottom right corner of the diagram in Figure 5.4 is connected to the input of the controller. The zero to twenty milli-amps current source in the diagram shown in Figure 5.5 is the current from the signal conditioner, which receives the equal zero to twenty milli-amps current from the output of the Eurotherm 808 controller. In the diagram shown in Figure 5.5, node IO1_2 is connected to the common ground of the circuit. The node IO1_1 is connected to the input of an operational amplifier shown in the top left corner of the diagram shown in Figure 5.4.

The diagram shown in Figure 5.6 is of the sub-circuit which simulates the disturbance injected into the plant when the switch is closed. The 1.5 volts supply across the resistor- capacitor sub-circuit of the SC2 sub-circuit diagram shown in Figure 5.6 is reduced, inverted twice, and subtracted from the voltage that enters the positive input of the differential amplifier from node IO1. The switch shown in the sub-circuit diagram in Figure 5.6 is closed at the designated time set in the configuration of the analog output

channel, channel one, of the data acquisition card with Simulink software. Analog output channel zero of the data acquisition card is reserved for the experiments of PI control at 60 hertz sample rate. The voltage at node IO1 is the output from the Sallen-Key architecture of the circuit diagram shown in Figure 5.4.

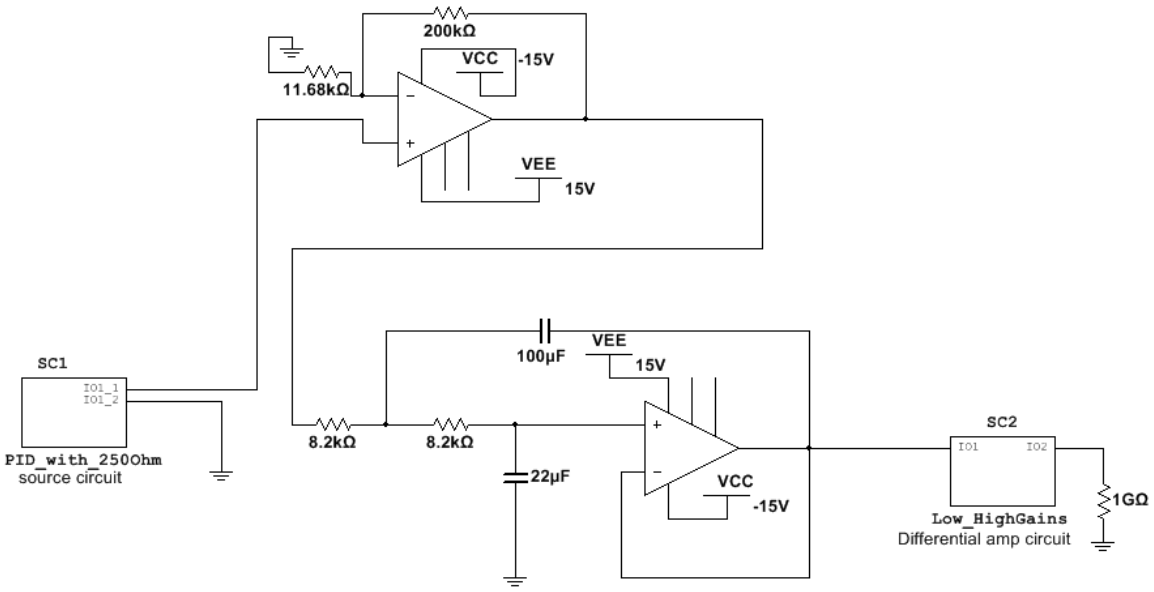

Figure 5.4 Electrical diagram of the plant.

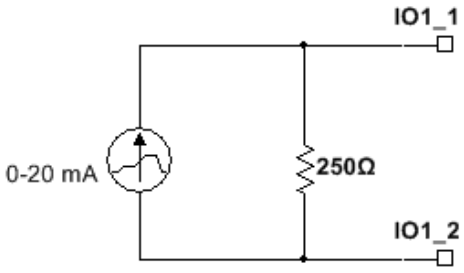

Figure 5.5 Electrical diagram of sub-circuit SC1 from Figure 5.4

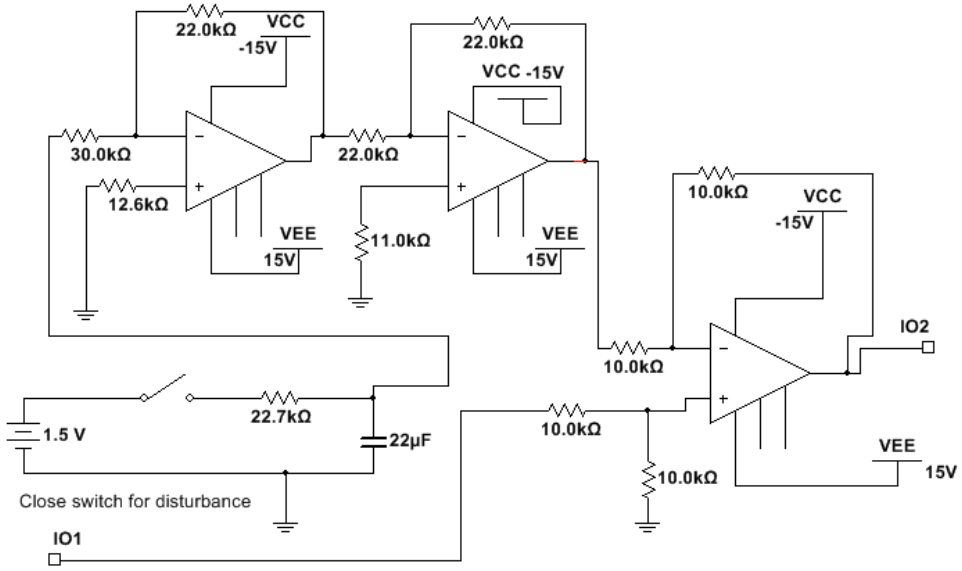

Figure 5.6 Electrical diagram of sub-circuit SC2 from Figure 5.4.

The primary constraint of the amplification used in the circuit that simulates the plant is the zero to ten volts range configuration of the input of the Eurotherm controller and the ten volts maximum voltage of the analog input channels of the data acquisition card. A photograph of the circuit is shown in Figure 5.7. Two sets of twisted pair red and black wires are at the output of the circuit. These pairs are the inputs of the controller and of the analog input channel of the data acquisition device. The black and white wires across the top of the board in this photo are the output wires of the signal conditioner. The one and a half voltage to the resistor-capacitor sub-circuit is connected at the bottom left corner of the circuit board. The connections to Va and Vb at the top of the circuit board are the positive fifteen and negative fifteen supply voltages, respectively, used to supply power to the operational amplifiers and the signal conditioner. The operational amplifiers are not in the same orientation on the circuit board. The buses along the frame of the circuit board are the common ground of the circuit.

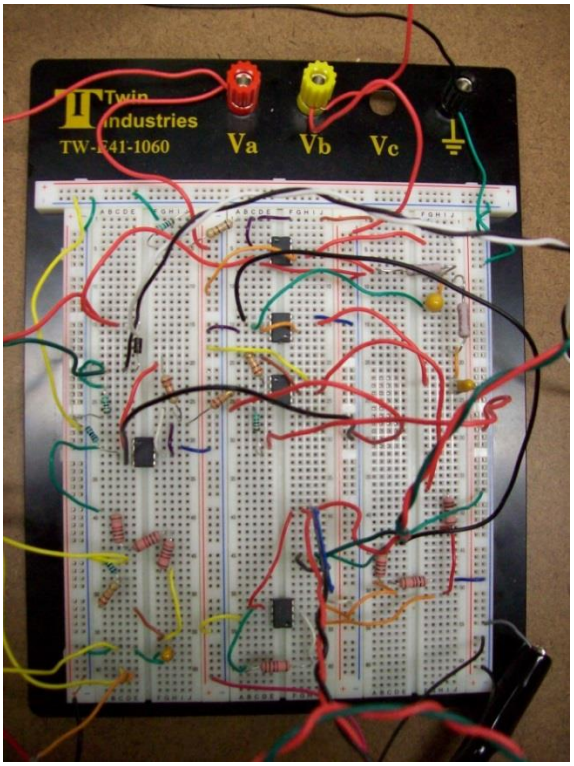

Figure 5.7 Photograph of the electrical circuit that is part of the experimental plant.

The set-up of the experiments with the Eurotherm controller for PI control at eight hertz consists of the circuit, Eurotherm controller, signal conditioner, and a Measurement Computing PCI-DAS1002 analog and digital multifunction card for data acquisition on a Vostro 200 computer with Matlab and Simulink software, along with Windows Real-Time for data acquisition. The one and a half volts supply to the resistor-capacitor sub-circuit is supplied by an analog output channel of the PCI-DAS1002 card through configuration with a Simulink model. A block diagram of the computer , analog card, and circuit used for the PI experiments at 60 hertz sampling rate is shown in Figure 5.9.

The power source for the amplifiers and the signal conditioner are shown in the far right corner of the white board upon which the circuit board is mounted. The same

hardware set-up, minus the Eurotherm controller and signal conditioner, is used for PI control at 60 hertz sampling rate. For the experiments of PI control at 8 hertz sampling rate, the Eurotherm controller is used, and its sampling rate is eight hertz. The analog input channels of the data acquisition card, channel zero and channel one, are configured in the Simulink model for 50 hertz sampling rate. Input channel zero collects the process variable voltage and input channel one collects the controller output voltage.

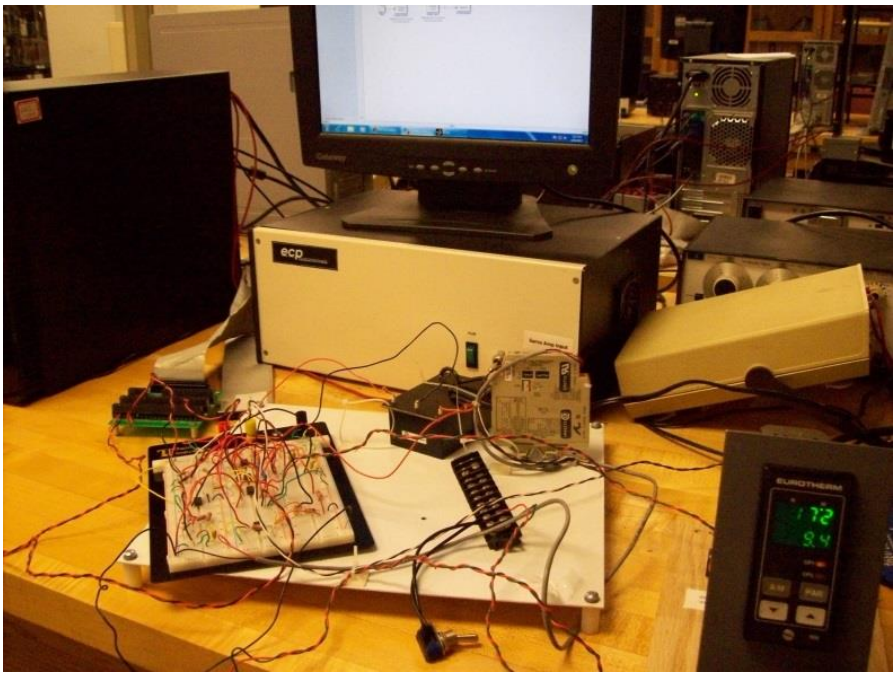

Figure 5.8 Set-up of the experiment of PI control at eight hertz sampling rate.

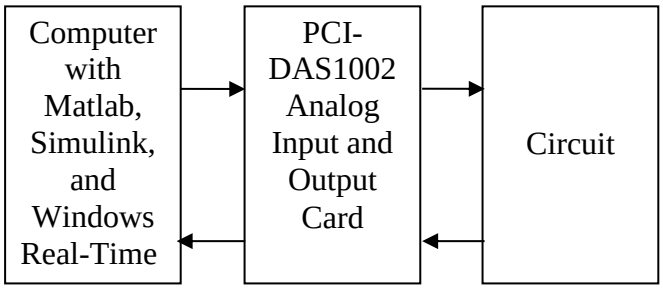

Figure 5.9 Block diagram of the experimental set-up for PI control at 60 hertz sampling rate.

Along with the configuration of the input signal as zero to ten volts in the menu of the Eurotherm controller, the process variable range is configured as one to two hundred fifty. The value of one is set as the minimum of this range to avoid an under range indication on the operator panel when the voltage input of the Eurotherm is a negative value or close to zero. The value of 250 at the maximum of this range allows for the set-point of 18,500 Pa-s simulated magnitude of the change in viscosity to be measured as approximately 7.39 to 7.41 volts by the Eurotherm input and appear as 185 on the user screen of the controller.

Equation 3.17 is re-stated here as Equation 5.1:

$$\ddot{y} = -2.6924\dot{y} - 6.4516y - 5990.23u \tag{5.1}$$

The design configurations of the Eurotherm controller along with the circuit design shown in Figure 5.4 results in a plant model design described by:

$$\ddot{y} = -2.439\dot{y} - 6.760y + 156.28u \tag{5.2}$$

where the natural frequency of the plant is 2.60 radians per second and the steady-state process gain is 23.12 change in process variable units per change in percent output of the controller. The process gain is equivalent to 18.1 volts output per volts input. The process gain for this experiment is positive due to the design of the circuit. Negative controller gains would be achieved by setting the control action direction parameter of the controller. The process variable set-point of 186 in this experiment means that this experiment simulates the regulation of viscosity to within 100 Pascal-seconds (10^2 Pa-s).

A voltage of 7.44 volts for a 186 process variable set-point means that a disturbance of 1600 Pa-s, or 16 process variable units, must be generated by a voltage of 0.64 volt. This would be accomplished with a battery voltage of 1.55 volts supplied to the resistor-capacitor sub-circuit. The gain amplifier and the Sallen-Key architecture along with the Eurotherm controller input, output, and process variable range configurations provide the experimental plant of (5.2).

A step response test of the system found that the process gain of the experimental plant is between 23 and 24 process variable units per percent output. An output of 7.9 percent output setting in manual mode is read by the Eurotherm controller as 185 process variable units. A volt meter verifies that a 7.9 percent output gives a voltage of 7.39 to 7.41 volts. It was verified that a 1.55 volts battery voltage supply to the resistor-capacitor sub-circuit with a closed switch will cause a reduction of 16 process variable units on the display screen of the Eurotherm controller during manual mode controller operation.

The PI controller gains used in simulation for (5.1) for a disturbance of 16,000 Pa-s, stated in Chapter IV, are K_P==-0.002247 and K_I =-0.0036660. The process gain of the plant model used in simulations of (5.1) is -928.488 pa-s per rpm. Due to the scaling of

the magnitude of the process gain in the experimental plant from 928 Pa-s per rpm to 23 process variable units per percent output, the PI controller gains determined through PI tuning described in Chapter IV could to be inversely scaled by the same value if the sampling rate of the PI control experiment were the same as the sampling rate of the simulations. This scaling value is approximately 40, therefore the starting point for selection of the gains of the PI controller for this experiment are:

$$K_{P\exp 1} = 40\left|K_{Psim}\right| = (40)(0.002247) = 0.09 \tag{5.3}$$

$$K_{I\exp 1} = 40\left|K_{Isim}\right| = (40)(0.003666) = 0.15 \tag{5.4}$$

The PI gains of the controller for this experiment will be positive because the process gain for this experiment is positive. The PI controller accepts the proportional gain in the form of the proportional band, X_P. The equation for the proportional band is:

$$X_P = \frac{100\%}{K_P} \tag{5.5}$$

The integral gain is accepted by the controller as an integer, in the form of integral time, τ_I , with units of seconds:

$$\tau_I = \frac{K_I}{K_P} \tag{5.6}$$

The proportional gain of 0.09 corresponds to a proportional band of 1110 percent. The integral time closest to the corresponding integral gain value of 0.15 in (5.4) for proportional gain 0.09 in (5.3) is two seconds. A closed-loop test of the Eurotherm 808 and the circuit, with X_P equal to 1110 percent and τ_I equal to two seconds, shows signs of instability without the disturbance added. This is expected because the Eurotherm 808

controller sample time is larger than the 0.01 second sample time used in the Simulink simulation of Chapter IV. The sample rate of the Eurotherm 808 is eight hertz.

A larger sample time requires a smaller proportional gain. The proportional band was increased to 2000 percent and the system was found to be unstable for the added disturbance of 16 process variable units. A proportional band of 3000 percent and an integral time of two seconds were selected in the controller menu of the Eurotherm controller.

For the experiments with the Eurotherm controller, a set-point of 185 process variable units is selected with the menu and arrows on the Eurotherm panel. Only an integer value of the process variable is allowed on the controller. The 185 process variable is approximately 7.4 volts measured by the Eurotherm controller. The Eurotherm controller is run in automatic mode for all experiments, with the system at steady-state at time equal to zero. The voltage from analog output channel zero of the data acquisition card is connected to the resistor-capacitor sub-circuit. This voltage is zero at time equal to zero. At time equal to eight seconds, the analog output channel one voltage is equal to 1.5 volts. As previously stated, the sampling rate of the process variable units by analog input channel zero of the data acquisition card is set to 50 hertz in the Simulink project. The experimental results are given in Section 5.2. The result of an open-loop step-input response test to a 0.62 volt disturbance input, resulting from the 1.5 volts input into the resistor-capacitor sub-circuit, is shown in Figure 5.10 for a constant controller voltage of 0.4 volt.

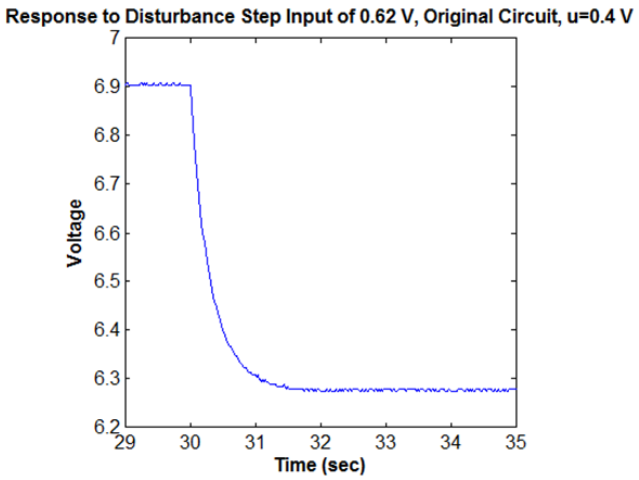

Figure 5.10 Open-loop response of the original circuit to 0.62 volt disturbance step input for a constant controller voltage of 0.4 volt.

The circuit is then changed to simulate a change in process gain and plant dynamics of the plant. The 8.2 kilo-ohms resistors of the Sallen-Key architecture were replaced with 10 kilo-ohms resistors The 11.68 kilo-ohms resistance, which is composed of an 11 kilo-ohms resistor in series with a 680 ohms resistor, was replaced with a ten kilo-ohm resistor in series with two 2.1 kilo-ohms resistors. The equation of the designed circuit with the change in process gain and dynamics in closed-loop with the Eurotherm controller with the same controller configurations as the first experiment is:

$$\ddot{y} = -2.00\dot{y} - 4.54y + 86.22u \tag{5.7}$$

where the natural frequency of the modified circuit is 2.13 radians per second and the steady-state process gain is 18.97 change in process variable units per change in percent output or 15.1 volts output per volts input. The process gain of the modified experimental plant is designed to be 86 percent of the original experimental plant process gain (5.2). The process gain of the inaccurately modeled plant is also 86 percent of the modeled

plant (5.1) in the simulations of Chapter IV. The designed natural frequency of the modified experimental plant is 82 percent of the designed natural frequency of the original experimental plant (5.2). In the simulations in Chapter IV, the natural frequency of the inaccurately modeled plant is 80 percent of the natural frequency of the modeled plant (5.1).

For PI control of the modified circuit at eight hertz sampling rate, the proportional band and integral time configurations of the controller were kept the same as the earlier experiment with the controller and the original circuit. At the beginning of the experiment, the analog output channel one voltage is zero so that no disturbance is injected into the plant. The process variable is at steady-state at time equal to zero. At time equal to eight seconds, the voltage of the analog output channel one is equal to 1.5 volts. The experimental results are given in Section 5.2.

For the experiments of PI control at 60 hertz sampling rate, a PI model in Simulink is used, with a configuration of a 60 hertz sampling rate of the analog input channel zero which is used as the input to the PI controller in the experiment, and a 60 hertz sampling rate of the output channel zero which is used as the output of the PI controller in the experiment. The analog output channel one is the 1.5 volts supply the resistor-capacitor sub-circuit, as was used for the first set of PI experiments. The Simulink model used for the PI experiments at 60 hertz is shown in Figure 5.11.

Results of experiments of PI control of the original circuit at 60 hertz sampling rate for a control voltage height equivalent to the control voltage height of the original circuit with ADRC at 60 hertz for a given set of ADRC tuning parameters are given in Section 5.4 for comparison with ADRC. The ADRC tuning parameters used in the ADRC and PI

comparison are specified in Section 5.3. The settings of the PI gains for the PI experiment with the original circuit at 60 hertz sampling rate is 0.400 for the proportional gain and 0.652 for the integral gain.

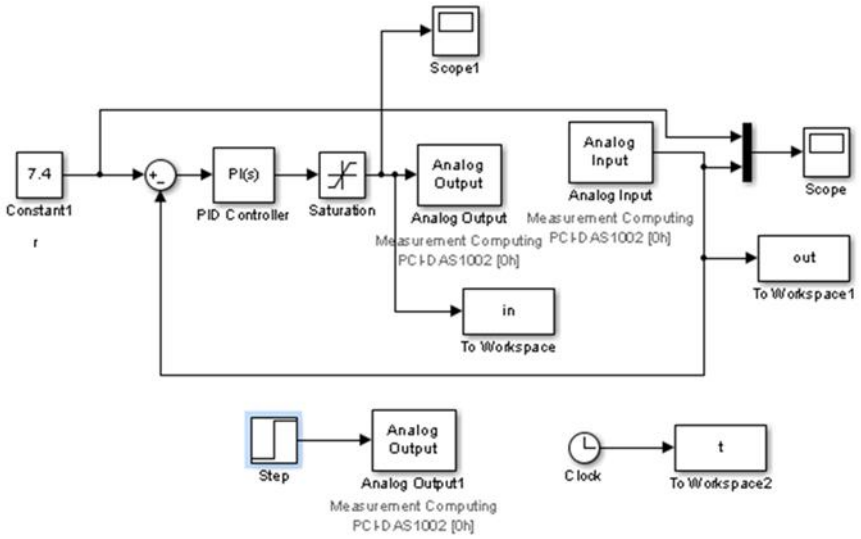

Figure 5.11 Simulink model used for PI experiments at 60 hertz sampling rate.

5.2 Experimental Results of PI Control

A proportional band of 3000 percent and integral time of two seconds configured on the Eurotherm 808 controller in closed-loop automatic control with the original circuit and with the modified circuit gives the results of the process variable voltages shown in

Figure 5.12 for a disturbance added to the system at time equal to eight seconds. A shorter time interval of the same data is shown in Figure 5.13. The process variable is at steady-state in closed-loop at time equal to zero. The process variable voltage and controller output voltage across the 250 ohms resistor are recorded at fifty hertz sampling rate. The controller sampling rate is eight hertz. The controller output voltage across the

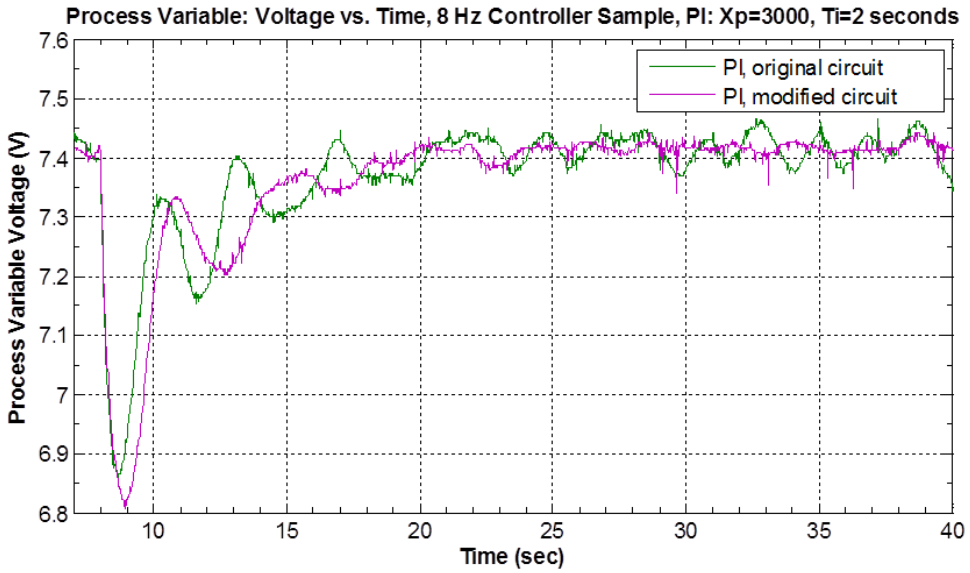

Figure 5.12 Process variable voltage versus time for 8 Hz with settings of X_P=3000 % and τ_I = 2 seconds with disturbance added at t=8 seconds.

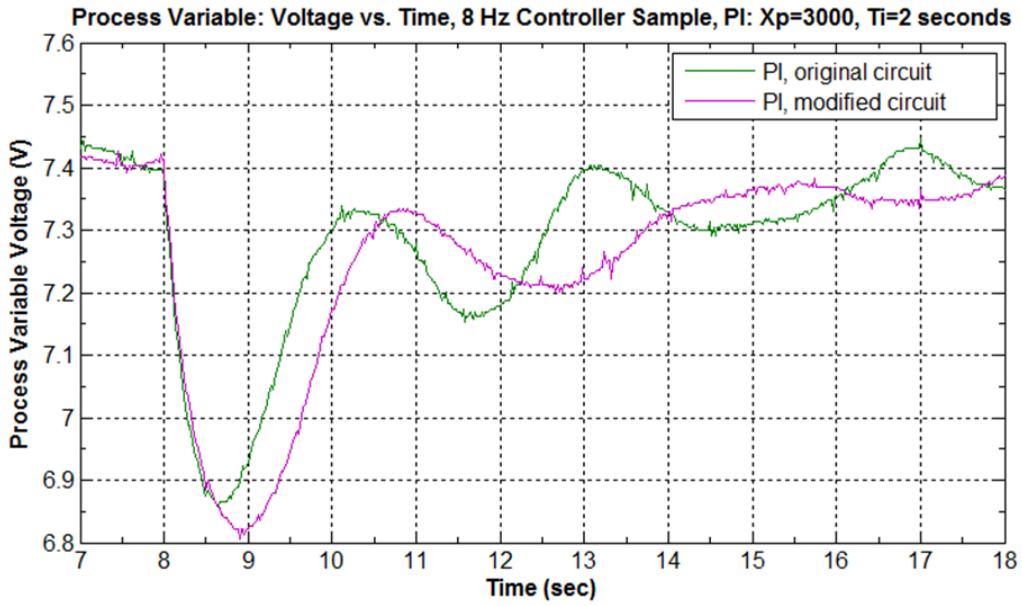

Figure 5.13 Process variable voltage versus time at 8 Hz for settings of X_P=3000 % and τ_I = 2 seconds with disturbance added at t=8 seconds, voltage to t=18 seconds.

250 ohms resistor for the original circuit and the modified circuit are shown in Figure 5.14.

In the experiment with the original circuit, the controller output ranges from 7.9 percent output to 8.5 percent output, which corresponds to the controller output voltage in Figure 5.14. In the experiment with the modified circuit, the controller output ranges from 9.5 percent output to 10.2 percent output to correspond to the controller output voltage shown in Figure 5.14.

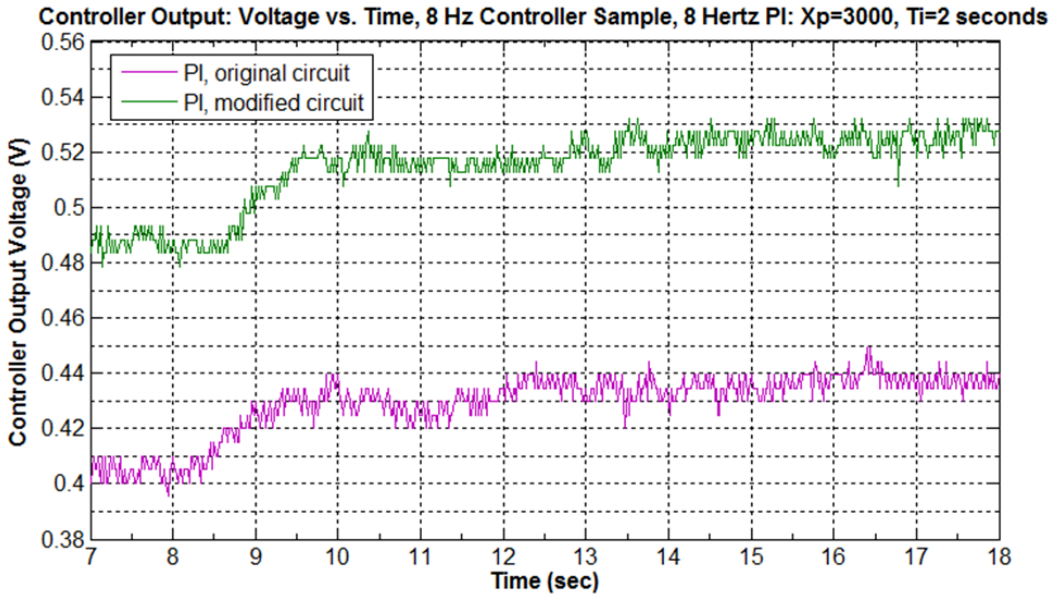

Figure 5.14 Controller voltage versus time at 8 Hz for settings of X_P=3000 percent and τ_I = 2 seconds with disturbance added at t=8 seconds.

The settling time of the process variable voltage to 7.3 volts, for the original circuit, is 4.5 seconds. The settling time of the process variable voltage to 7.3 volts, for the modified circuit, is 5.6 seconds. A process variable voltage of 7.3 volts for the Eurotherm controller configuration corresponds to a process variable of approximately 183 process variable units. The set-point of the experiment is 185 process variable units as set on the Eurotherm controller, which simulates a set-point of 18,500 Pa-s. In the Chapter IV simulations, the PI settles to within 200 Pa-s of the set-point in two seconds for the accurately modeled plant, and within 2.4 seconds for the inaccurately modeled plant. The settling time of the experiment is due to the larger sampling time of 0.125 second compared to the simulation sampling time of 0.01 second, and the choice of values for the proportional band and integral time for the settings of the Eurotherm controller. The

ratio of K_I/K_P of the gains chosen in simulation of the PI controller is 1.632, but the ratio of K_I/K_P for the PI experiments with the Eurotherm controller is two. As stated in Section 5.1, this ratio is due to the requirement by the Eurotherm controller of an integer value for the integral time setting.

The maximum error of the process variable is approximately 16 process variable units for closed-loop of the PI controller with the original circuit and the modified circuit at eight hertz sampling rate. The 15 process variable value corresponds to 1500 Pa-s. This error is larger than the maximum errors of 600 Pa-s and 700 Pa-s determined in the simulations in Chapter IV for the original and modified plant, respectively, as seen clearly in Figure 4.2. Comparison of the controller voltages shown in Figure 5.13 for both circuits is inconclusive of a difference in oscillation of the control law between the original circuit and the modified circuit.

The height of the steady-state controller output voltage signal is approximately 0.007 volt. This value was used to select the ADRC parameter gains of the controller and observer bandwidth that would result in the same steady-state controller output voltage height, which is an of comparable controller action. Section 5.3 describes the set-up of the ADRC experiments. The results of the PI experiment at 60 hertz sampling rate are given in Section 5.4 for comparison with the experiments of ADRC at 60 hertz.

5.3 Experimental Set-Up of ADRC

The same hardware set-up that was used for the PI experiments, minus the Eurotherm controller and signal conditioner, was used for experiments of ADRC with the same original and modified circuits described in Section 5.1. The input measurement and output signals of the data acquisition card are each a voltage. The process gain of the original circuit is the steady-state voltage output gain for a voltage input, which is 18.1.The process gain of the modified circuit is 15.1 volts output per volts input.

Analog input channel zero is used to measure the voltage at the one giga-ohm resistor on the circuit board. This voltage is the input to the ADRC controller in the Simulink model. Analog output channel zero is the output of the ADRC controller, in volts, across the 250 ohms resistor on the circuit board. Analog output channel one is the voltage applied to the resistor-capacitor sub-circuit of Figure 5.6. The sampling rate of the data acquisition channels and the Simulink model in the first set of ADRC experiments with the original and modified circuits is eight hertz. The voltage of the analog output channel one from time zero until time prior to 40 seconds is zero. At time equal to 40 seconds, analog output channel one voltage is 1.5 volts. A set-point of 7.4 volts is designated in the ADRC experiment, which is equivalent to the 185 process variable set-point of the PI experiments at eight hertz with the Eurotherm controller. The Simulink model used in the ADRC experiments is shown in Figure 5.15.

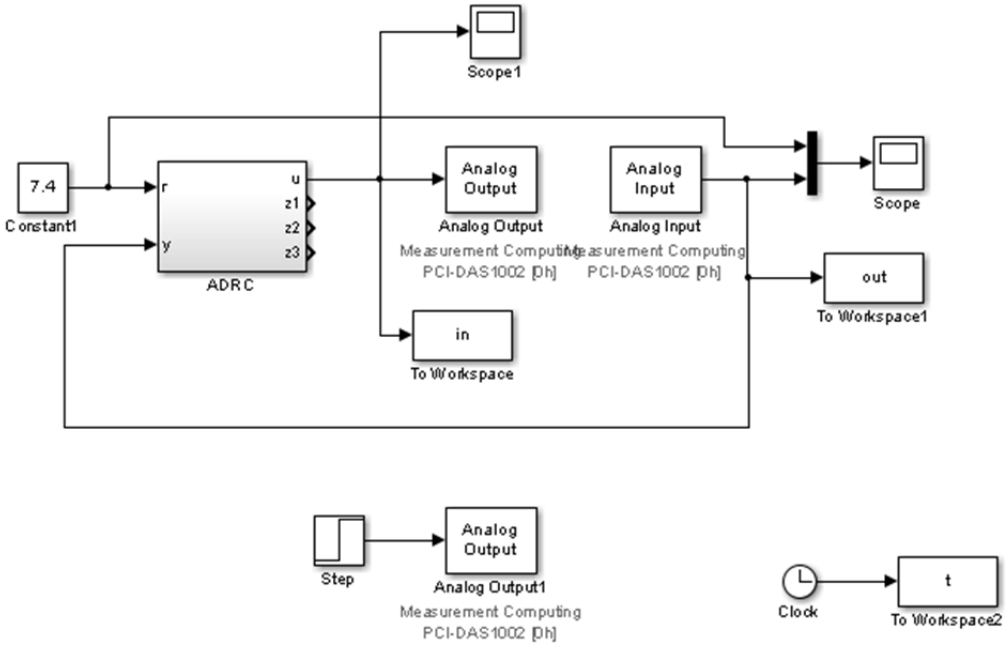

Figure 5.15 Simulink model used in ADRC experiments.

The Simulink model of the ADRC controller used in this experiment is shown in Figure 5.17. A saturation limit of 0.8 volt is set on the output of the ADRC controller to keep the process variable voltage below the maximum level of the analog input channel of the data acquisition card, which is 10 volts.

Different parameter gains for controller and observer bandwidth were used with b_0 parameter setting of 125 until an approximate value of 0.007 volt in steady-state controller output voltage was achieved. The observer bandwidth of 7.00 radians per second and controller bandwidth of 2.25 radians per second were found to achieve approximately 0.007 volt height in controller output action. Experiments for b_0 values of 125 and 200 were conducted with the original circuit and the modified circuit, respectively. The results of the experiments are given in Section 5.4 with a comparison to the PI experiments.

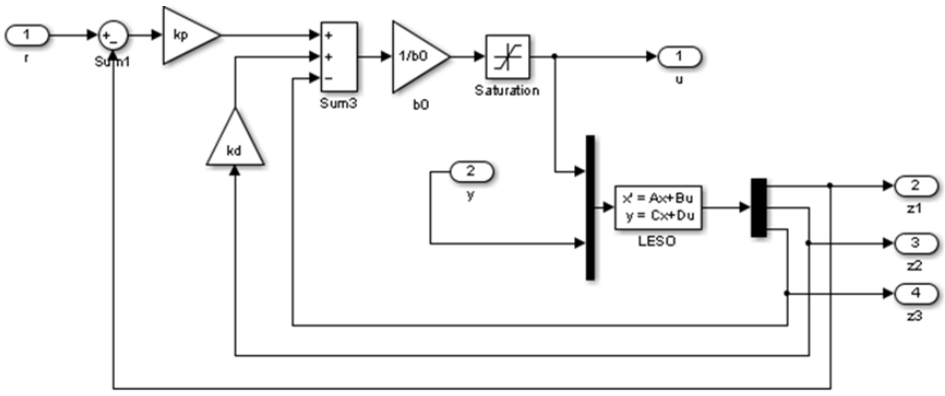

Figure 5.16 Simulink model of ADRC controller used in experiments.

5.4 Experimental Results of ADRC and Comparison With PI

The process variable voltage and controller output voltage results of the ADRC experiments at eight hertz sampling rate are given in Figure 5.18 and Figure 5.19, respectively. The disturbance is introduced at time equal to 40 seconds. The process variable voltage and controller output voltage from the PI experiments at eight hertz, shown in Figure 5.13 and Figure 5.14, respectively, are overlaid on the ADRC plots. This is accomplished with the plot function of Matlab with an increase of 32 seconds to the time variable of the PI data, since the disturbance is added at time equal to eight seconds in the PI experiments compared to the disturbance added at time equal to 40 seconds for the ADRC data.

The data acquisition sampling rate of the analog input channel of the analog card is 50 hertz for the PI experiment, though the sampling rate of the PI controller is eight hertz.

For the ADRC experiments, the sampling rate of the analog input and output channels of the analog card for the ADRC experiments is eight hertz.

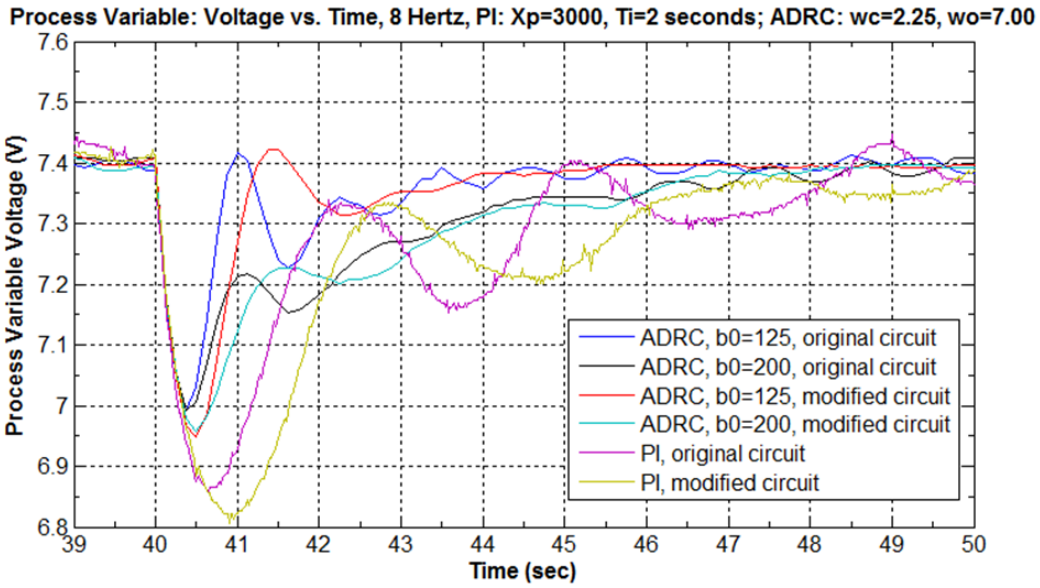

Figure 5.17 Process variable voltage versus time for ADRC experiments at 8 Hz sample rate with disturbance added at t=40 seconds, compared to PI.

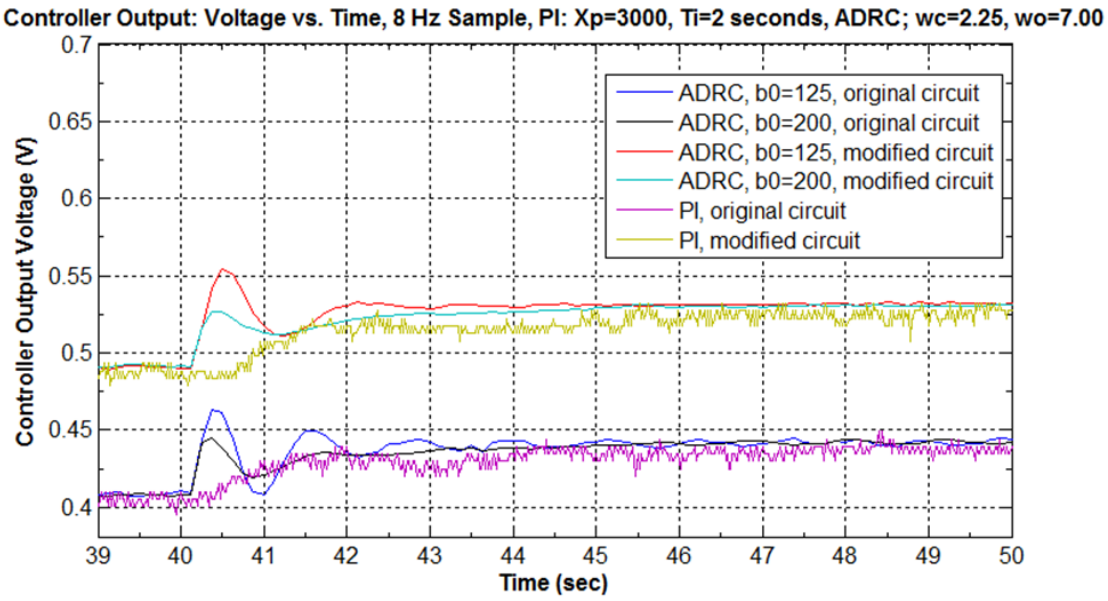

Figure 5.18 Controller output voltage versus time for ADRC experiments at 8 Hz sample rate with disturbance added at t=40 seconds, compared to PI 8 Hz controller sample rate with 50 Hz data acquisition of analog card for PI experiment.

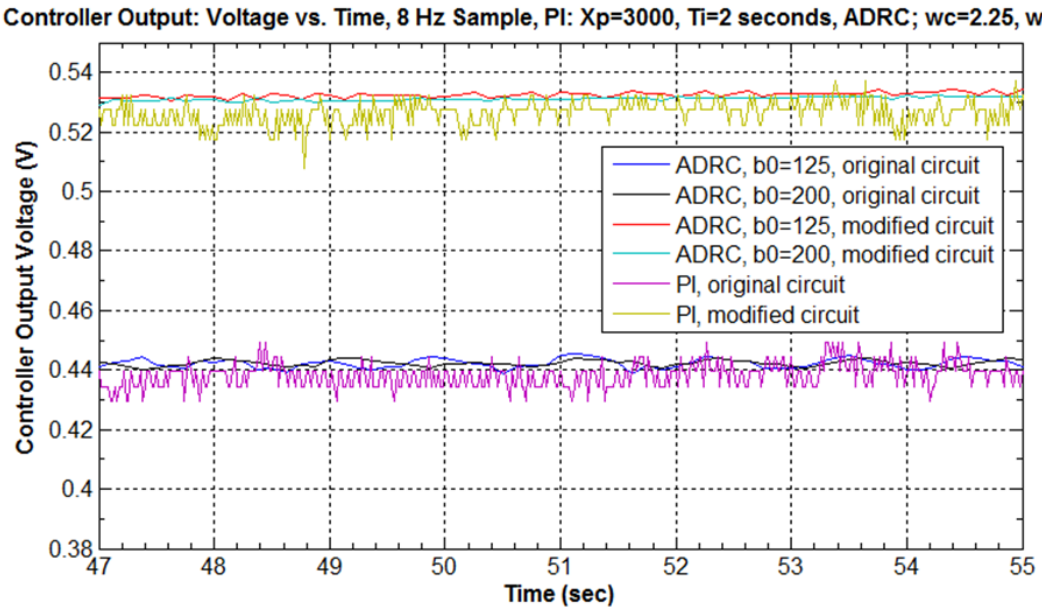

Figure 5.19 Comparison of height of controller output voltages of PI and ADRC at 8 Hz with 50 Hz data acquisition of analog input card for PI experiment.

Figure 5.20 and Figure 5.21 show a small discrepancy in the controller voltage at steady-state for both circuits. This discrepancy is approximately 0.05 volt and is due to the setting of the integer value of the process variable as 185 on the Eurotherm controller, which is as close to 7.4 volts as possible. From Figure 5.18, it can be seen that the settling time for ADRC to within 0.1 volts of the set-point is less than 4 seconds for all experiments, compared to 4.5 seconds for PI control of the original circuit and 5.6 seconds for PI control of the modified circuit at 8 hertz, for b_0 range of 125 to 200, for controller bandwidth, ω_c, of 2.25 radians per second and observer bandwidth, ω_o, of 7.00 radians per second. The b_0 value of 200 is approximately the same scale to the 9000 magnitude value of b_0 used in the simulation as the process gain of the circuit in the experiment to the process gain of the plant used in simulation, considering that the process gain of the original circuit is 18.1 volts output to volts input. The ADRC provides faster settling time and lower initial error for the same controller output voltage height at steady-state and the same controller sampling frequency.

The controller output voltage for the ADRC experiment with the original circuit at 60 hertz sampling rate, and settings of b_0 of 150, controller bandwidth, ω_c, of 6.3 radians per second and observer bandwidth, ω_o, of 19.0 radians per second are shown in Figure 5.21 with PI at 60 hertz and proportional gain and integral gain settings for the same height of control action as the ADRC. These PI gains are 0.400 for the proportional gain and 0.652 for the integral gain. The same height of control action for ADRC and PI is seen in Figure 5.21. The corresponding process variable voltage is shown in Figure 5.22. It can be seen by the oscillations with PI control in Figure 5.22 that the control system for these PI gains are unstable. For the same sampling frequency and control

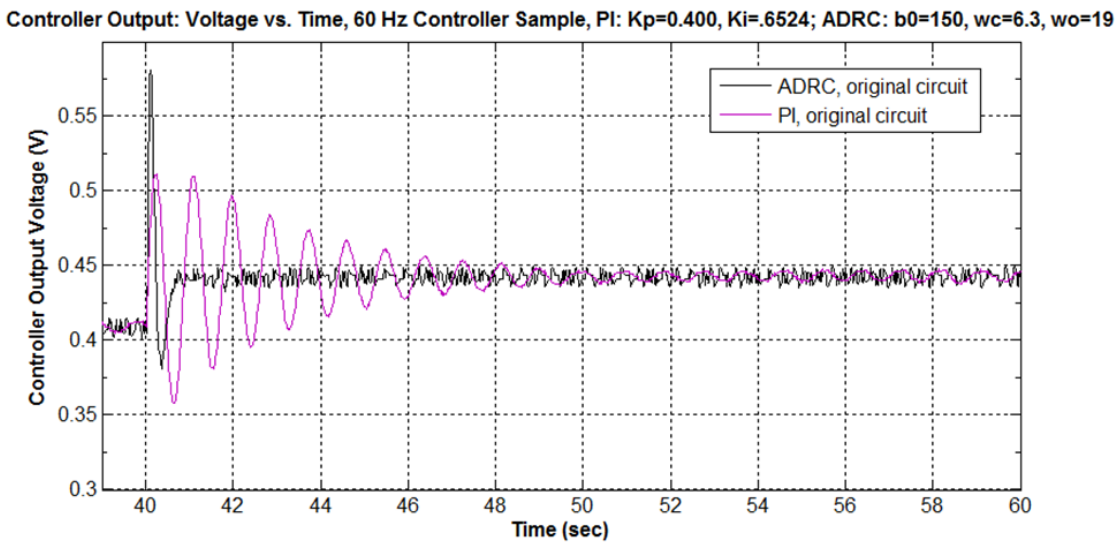

Figure 5.20 Controller output voltage for ADRC and PI at 60 Hz for same controller action.

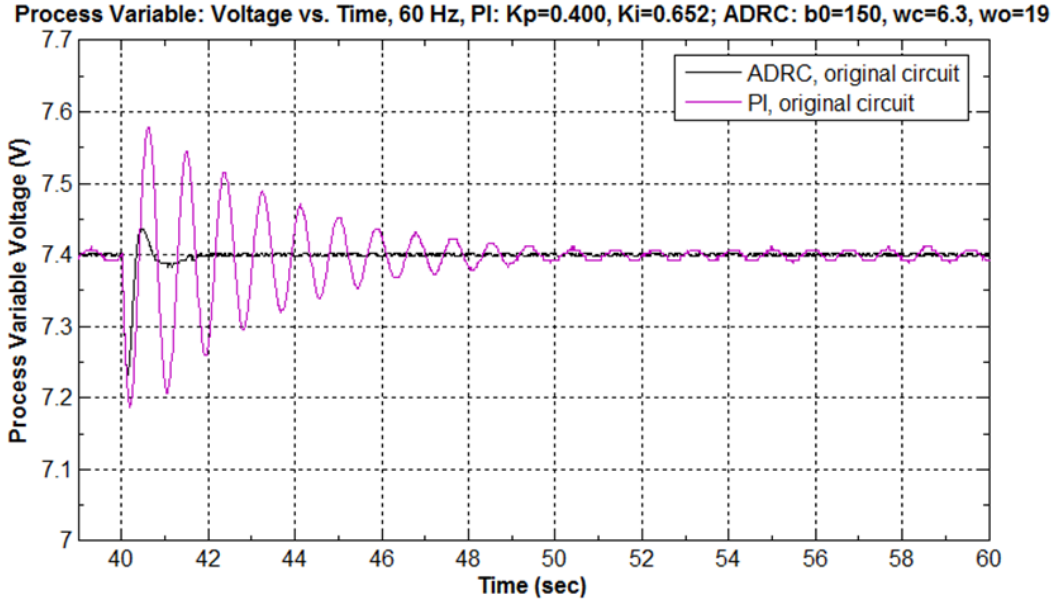

Figure 5.21 Process variable voltage for ADRC and PI at 60 Hz for same controller action.

voltage height, the ADRC has a faster settling time of the output, less oscillation of the control signal, and a larger margin of stability.

CHAPTER VI

CONCLUSIONS AND FUTURE WORK

An easily applicable first principle model for viscosity regulation in polymer extrusion does not exist. The ability to close the loop is perceived by researchers and industry as difficult because of the complexity of the process. Researchers have proposed different forms of the PID for viscosity regulation. The gains of these PID and PI controllers are tuned for specific polymer grades, equipment, and operating conditions. There is a definite cost savings that can be accomplished by closing the loop with an advanced method that can be applied easily in industry.

This thesis is an initial investigation of control in polymer extrusion, in which the problem of viscosity regulation is reformulated as a disturbance rejection problem. This is very significant because it verifies that a general approach exists for easier and faster set-up of a controller on an extrusion line. It may also be possible to use one ADRC algorithm to regulate viscosity for several grades of the same polymer on the same extruder. Regulation during the likelihood of disturbances in coupled variables and

changes in properties of continuously fed ingredient materials is a necessity in polymer extrusion to maintain the required product quality. ADRC provides effective quality control, and rejects disturbances faster than traditional PID.

Simulations of ADRC and PI control were presented and compared. Experiments with ADRC and PI each in closed-loop with a circuit simulating a second order extrusion process with screw speed manipulation and an injected disturbance due to ingredient grade property change validated the results of the ADRC simulation.

The conclusions of this thesis are given in Section 6.1. The future work is discussed in Section 6.2.

6.1 Conclusions

A new approach to viscosity regulation in polymer extrusion is needed. PI and PID controllers are the prevalent form of control used in the polymer industry, though an operator may control some part of the process based on visual inspection. The operator control still exists in the industry because it is impossible to generate an accurate model of the process. This thesis provides validation that there is an alternative for control in the extrusion process beyond PID, without the need for an accurate model.

Viscosity regulation is prone to disturbances and changes in dynamics. It was shown in simulations of a disturbance added to an inaccurately modeled system that the traditionally tuned PI brought the viscosity back to set-point but with more viscosity oscillation, longer settling time, and higher initial error than with ADRC. This was

validated with comparison of results from ADRC and PI control of a plant-simulating circuit hardwired to an industrial controller and to a personal computer with Matlab, Simulink, and Windows Real-Time. Also, for the same sampling rate and equivalent controller output signal height, it was shown that the margin of stability is higher for ADRC.

Most significantly, the accuracy of the model was not required for ADRC to provide effective control. This was shown in simulation and verified through experimental results of ADRC by the range of values chosen for the b_0 parameter in the experiments in scale to the b_0 parameter chosen in simulation equal to the scale of the process gain of the plant circuit of the experiment to the process gain used in the plant of the simulation. Based on the experimental results of this initial study, ADRC is a good solution to viscosity regulation in polymer extrusion.

6.2 Future Work

The method of ADRC regulates processes without requiring an accurate model. The use of ADRC in polymer extrusion for disturbance rejection and effective viscosity regulation would not be a difficult task to implement on extrusion equipment with a programmable logic controller (PLC). Hardware requirements are a PLC with a computer processing unit (CPU) that has enough memory to hold variables and perform calculations. These calculations include derivatives and integrals. The CPU is required, along with a power supply, an analog input module and an analog output module. A communication module is required in the PLC chassis if the signals to or from the input

and output modules are not current or voltage. There must also be a hardware port for connection of a cable to a computer so that the program may be uploaded to the CPU. The specific CPU cable for uploading programs from the computer is also required. If operator communication with the PLC program is necessary, for example in switching from start-up of the extruder to automatic control, then a human machine interface (HMI) panel or a digital input module with push buttons are also required.

Software requirements for ADRC include the programming software that is manufacturer specific to the PLC. For example, an Allen Bradley controller would require RSLogix software specified version for the PLC. An HMI panel would also require programming software, which may also be manufacturer specific. The PLC and HMI programming software should be on a computer that can connect to the PLC while it is in the operator panel. The programming software must allow the programmer to write code in text commands. This is necessary for construction of calculation commands, array management, and use of loops and counters of the ADRC algorithm in discrete form.

The experimentation of ADRC on an extrusion line to investigate its effectiveness for viscosity regulation would be the next task for future work. Along the same lines as viscosity regulation in polymer extrusion, ADRC implementation for mold quality regulation in blow molding and injection molding processes would also be an area of interest for future research. The simulation and experimental results of this thesis provides the first glimpse of the applicability of ADRC to viscosity regulation in polymer extrusion. Future work that involves ADRC implementation on extrusion equipment will add knowledge from industrial case studies to this body or work.

REFERENCES

[1] F. Previdi, S. M, Savaresi, and A. Panarotto, "Design of a feedback control system for real-time control of flow in a single-screw extruder," *Control Engineering Practice*, vol. 14, pp. 1111-1121, 2006.

[2] M. Del Pilar Noriega, E. and C. Rauwendaal, Troubleshooting the extrusion process: a systematic approach to solving plastic extrusion problems, Hanser, Munich, 2001.

[3] P. E. Wellstead, W. P. Health, and A. P. Kjaer, "Identification and control of web processes; polymer film extrusion," *Control Engineering Practice*, vol. 6, pp. 321-331, 1998.

[4] A. K. Kochhar and J. Parnaby, "Dynamic modeling and control of plastics extrusion processes," *Automatica*, Vol. 13, pp. 177-183, 1977.

[5] M. H. Costin, P. A. Taylor, and J. D. Wright, "A critical review of dynamic modeling and control of plasticating extruders," *Polymer Engineering and Science*, vol. 22, no. 7, pp. 393-401, 1982.

[6] B. Yang and L. J. Lee, "Process control of polymer extrusion, Part I: feedback control," *Polymer Engineering and Science*, vol. 26, no. 3, pp. 197-204, 1986.

[7] M. McAfee, "Enhancing process insight in polymer extrusion by grey box modeling," *Trans. of the Inst. of Measurement and Control*, vol. 29, no. 5, pp. 467-488, 2007.

[8] X. Liu, K. Li, M. McAfee, B. K. Nguyen, and G. M. McNally, "Dynamic gray-box modeling for on-line monitoring of polymer extrusion viscosity," *Polymer Engineering Science*, vol. 52, no. 6, pp. 1332-1341, 2012.

[9] L. Tan, A. Lofti, E. Lai, and J. B. Hull, "Soft computing applications in dynamic model identification of polymer extrusion process," *Applied Soft Computing*, vol. 4, pp. 345-355, 2004.

[10] T. O. Broadhead, W. I. Patterson, and J. M. Dealy, "Closed loop viscosity control of reactive extrusion with an in-line rheometer," *Polymer Engineering and Science*, vol. 36, no. 23, pp. 2840-2851, 1996.

[11] S. Chiu and S. Pong, "In-line viscosity control in an extrusion process with a fuzzy gain scheduled PID controller," *Journal of Applied Polymer Science*, vol. 74, pp. 541-555, 1999.

[12] A. Pabedinskas, W. R. Cluett, and S. T. Balke, "Process control for polypropylene degradation during reactive extrusion," *Polymer Engineering and Science*, vol. 29, no. 15, pp. 993-1003, 1989.

[13] A. Pabedinskas and W. R. Cluett, "Controller design and performance analysis for a reactive extrusion process," *Polymer Engineering and Science*, vol. 34, no. 7, pp. 585-597, 1994.

[14] S. Chiu and S. Pong, "In-line viscosity fuzzy control," *Journal of Applied Polymer Science*, vol. 79, no. 7, pp. 1249-1255, 2000.

[15] E. L. Steward, "Control of melt temperature on single screw extruders," *SPE-ANTEC Technical Papers*, 1999.

[16] C. Rauwendaal, *Polymer Extrusion, 3rd ed*., Hanser Verlag, Munich, 1994.

[17] http://en.wikipedia.org/wiki/Extrusion.

[18] G. L. Bata, "The Archimedean screw as an extruder; historical note," *Polymer Engineering and Science*, vol. 24, no. 9, pp. 624-625, 1984.

[19] Q. Zheng and Z. Gao, "An energy saving, factory-validated disturbance decoupling control design for extrusion processes," *10th World Conference on Intelligent Control and Automation*, IEEE, Beijing, pp. 2891-2896, 2012.

[20] Z. Chen, P. Chao, S. Chiu, "Proposal of an empirical viscosity model for quality control in the polymer extrusion process," Poly. Testing, 22, pp.601-607, 2003.

[21] M. Xanthos, *Reactive Extrusion: Principles and Practice*, Hanser Verlag, Munich 1992.

[22] K. J. Ganzeveld, L. P. B. M. Janssen, "Role of mixing and rheology in reactive extrusion," *Ind. Eng. Chem. Res*., vol. 33, pp. 2398-2403 1994.

[23] Z. Tadmor, "Dynamic Model of a Plasticating Extruder," *Polymer Engineering and Science*, vol. 14, no. 2, pp. 112-119, 1974.

[24] J. L. White, *Rubber Processing: Technology, Materials, and Principles*, Carl Hanser Verlag, Munich, pp. 162-211, 1995.

[25] M. Faraday, *The London, Edinburgh, and Dublin Philosophical Magazine and Journal of Science*, vol. 32, pp. 165-167, 1848.

[26] M. Gray, British Patent (filed Dec. 10, 1879) 5,056, 1880.

[27] J. L. White, H. Potente, and U. Berghaus, *Screw Extrusion: Science and Technology*, Carl Hanser Verlag, Munich, pp. 1-5, 2003.

[28] V. E. Royle, U.S. Patent (filed June 4, 1929) 1,904,884, 1933.

[29] N. C. Lee, *Understanding Blow Molding, 3rd ed*., Hanser Verlag, Munich, 2007.

[30] Z. Tadmor, "Polymer processing technology to science and technology," *Plastics Engineering, Transcript from SPE-ANTEC 1994*, 1994.

[31] B. H. Maddock, *SPE Journal*, vol. 15, p. 383, 1959.

[32] J. Han, "Auto-disturbance rejection control and its applications," *Control and Decision*, vol. 13, no. 1, pp. 19-23, 1998 (In Chinese).

[33] J. Han, "Nonlinear design methods for control systems," *Proceedings of the 14th IFAC World Congress*, Beijing, 1999.

[34] Z. Gao, "Scaling and parameterization based controller tuning," *Proceedings of the American Control Conference*, Denver, pp. 4989-4996, 2003.

[35] R. C. Dorf, R. H. Bishop, *Modern Control Systems, 10th Edition*, Prentice Hall, Upper Saddle River, 2005.

[36] http://www.search-document.com/pdf/1/eurotherm-808-controller-manual.html.

[37] C. Jun, Z. Dongzhi, Y. Yanjuan, "Model prediction and numerical simulation of melt temperature distribution in process of polymer extrusion," *IEEE International Conference on Intelligent Computing and Intelligent Systems*, vol. 2, pp. 808-812, 2009.

[38] X. Liu, K. Li, M. McAfee, and J. Deng, "Soft-sensor for real-time monitoring of melt viscosity in polymer extrusion process," *Proceedings of the 49th IEEE Conference on Decision and Control*, Atlanta, pp. 3469-3474, 2010.

[39] P. A. Balakrishnan and S. Ravi, "Design of intelligent self tuning ANFIS temperature controller for plastic extrusion process," *IEEE International Conference on Communication Control and Computing Technologies*, Ramanathapuram, pp. 314-320, 2010.

[40] G. Tian and Z. Gao, "Frequency response analysis of active disturbance rejection based control system," *Proceedings of the 16th IEEE International Conference on Control Applications, Part of IEEE Multi-Conference on Systems and Control*, Singapore, pp. 1595-1598, 2007.

[41] Q. Zheng, Z. Chen, and Z. Gao, "A practical approach to disturbance decoupling control," *Control Engineering Practice*, vol. 17, no. 9, pp. 1016-1025, 2009.

[42] Z. Gao, Y. Huang, and J. Han, "An alternative paradigm for control system design," *Proceedings of the 40th IEEE Conference on Decision and Control*, Orlando, pp. 4578-4585, 2001.

[43] Z. Gao, "Active disturbance rejection control: a paradigm shift in feedback control design," *Proceedings of the American Control Conference*, Minneapolis, pp. 2399-2405, 2006.

[44] J. Han, "From PID to active disturbance rejection control," *IEEE Transactions on Industrial Electronics*, vol. 56, no. 3, pp. 900-906, 2009.

[45] Y. Huang, K. Xu, J. Han, and J. Lam, "Flight control design using extended state observer and non-smooth feedback," *Proceedings of the 40th IEEE Conference on Decision and Control*, Orlando, pp. 223-228, 2001.

[46] "Linestream Technologies: Advanced Control, Made Simple," Ohio Polymer, http://polymerohio.org.

[47] G. Walsh, D. Bigio, J. Gao, and P. Elkouss, "Viscosity regulation for polymer extruders," *SPE-ANTEC Technical Papers*, 2001.

[48] H. P. Tsoi and F. Gao, "Control of injection velocity using a fuzzy logic rule-based controller for thermoplastics injection molding," *Polymer Engineering and Science*, vol. 39, no. 1, pp. 3-17, 1989.

[49] Y. Yang, K. Yao, and F. Gao, "Design of an advanced injection molding control system," *SPE-ANTEC Technical Papers*, 2010.

[50] R. W. Diraddo and A. Garcia-Rejon, "On-line prediction of final part dimensions in blow molding: a neural network computing approach," *Polymer Engineering and Science*, vol. 33, no. 11, pp. 653-664, 1993.

[51] M. Wan and A. I. Isayev, "Injection molding of rubber compound with rheology affected by vulcanization: Part II modeling and experiment," *Rubber Chemistry and Technology*, vol. 69, no. 2, pp. 294-312, 1996.

[52] Z. Chen, L. Turng, "Advances in injection molding process/quality control," *SPE-ANTEC Technical Papers*, 2004.

[53] Z. Chen, L. Turng, "Adaptive online quality control for injection-molding by monitoring and controlling mold separation," *Polymer Engineering and Science*, vol. 46, no. 5, pp. 569-580, 2006.

[54] C. Koolhiran, J. L. White, "Comparison of intermeshing rotor and traditional rotors of internal mixers in dispersing silica and other fillers," *Journal of Applied Polymer Science,* vol. 78, pp. 1551-1554, 2000.

[55] A. Jain, N. Gupta, A. Nagpal "Effect of dynamic cross-linking on melt rheological properties of polypropylene/ethylene-propylene-diene rubber blends," *Journal of Applied Polymer Science,* vol. 77, pp. 1488-1505, 2000.

[56] A. Healy, R. Dubay, A. Gerber, "Controlling melt temperature in injection molding using an adaptive CFD predictive controller," *SPE-ANTEC Technical Papers,* 2003.

[56] http://switzernet.com/people/emin-gabrielyan/060531-from-1st-transatlantic-to-arpanet/trans27atlantic/cache/Gutta-Percha.htm.

[58] http://www.atlantic-cable.com/Article/GuttaPercha/.

[59] D. W.Bartlett, *London by Day and Night,* pp. 56-59, 1852.

[60] http://dssmhi1.fas.harvard.edu/emuseumdev/code/emuseum.asp?action=advsearch&newsearch=1&profile=people&rawsearch=constituentid/,/is/,/6666/,/false/,true&style=single&searchdesc=Gutta%20Percha%20Company.

[61] R. A. Brooman, H. Brewley, English Patent 10,582, 1845.

[62] F. H. Banbury, U.S. Patent (filed Jan. 15, 1916) 1,200,070, 1916.